

THE EFFECTS OF IRON CARBONYL-BASED CATALYST PRECURSORS ON THE REACTION OF 4-(NAPHTHYLMETHYL)BIBENZYL

Timothy D. Walter, Stephen M. Casey, Michael T. Klein, Henry C. Foley
Center for Catalytic Science and Technology
Department of Chemical Engineering
University of Delaware
Newark, DE 19716

ABSTRACT

The reaction pathways and kinetics of 4-(naphthylmethyl)bibenzyl (NBBM) were studied in an effort to resolve certain fundamentals underlying catalysis of coal liquefaction by Fe-based catalysts. Reaction of NBBM under a hydrogen atmosphere was performed for a series of iron carbonyl-based catalyst precursors: $\text{Fe}(\text{CO})_4\text{PPh}_3$, $\text{Fe}(\text{CO})_3(\text{PPh}_3)_2$, and $\text{Fe}(\text{CO})_2(\text{PPh}_3)_2\text{CS}_2$. The precursors' activities for the disappearance of NBBM were $\text{Fe}(\text{CO})_4\text{PPh}_3 > \text{Fe}(\text{CO})_2(\text{PPh}_3)_2\text{CS}_2 > \text{Fe}(\text{CO})_3(\text{PPh}_3)_2$. All precursors gave significantly higher rates than that for thermal reaction at 400°C. Thermolysis of NBBM was selective for cleavage at the bibenzyl bond, whereas the catalyst precursors were selective for cleavage at the naphthyl moiety. Hydrogenation activity was also observed for each of the three catalyst precursors. Possible catalytic reaction mechanisms are considered.

INTRODUCTION

Direct coal liquefaction is the process of fragmenting the coal structure into lower molecular weight materials. Thermal liquefaction is accompanied by bond-making retrograde reactions, which can result in a more refractory solid than the original coal. This poor thermal selectivity to desirable products motivates the use of a catalyst to increase the rate and selectivity of liquefaction.

Much of the microporous coal structure¹ is not accessible to classical solid catalyst particles. This suggests that the use of homogeneous or fine particle catalysts, which would better access the pore structure and, in turn, the surface area of coal, could be promising for catalysis of coal reactions. The two key coal liquefaction reaction families of bond scission and hydrogenation could thus occur for coal, and not only coal-derived liquids.

Our continuing work has focused on iron-based materials. In particular, catalyst precursors that are able to form fine particle iron and iron sulfides at coal liquefaction conditions have been sought. To consider the effect of the precursor's ligands on the activity of the catalyst, the series $\text{Fe}(\text{CO})_4\text{PPh}_3$, $\text{Fe}(\text{CO})_3(\text{PPh}_3)_2$, and $\text{Fe}(\text{CO})_2(\text{PPh}_3)_2\text{CS}_2$ of triphenylphosphine (PPh₃)-substituted iron carbonyls has been examined.

The evaluation of these catalysts involved extensive model compound reaction chemistry. This is because simple model systems, individually, mimic some of the important structural features in coal, which enables the examination of specific bond reactivities in coal. The use of well-defined hydrocarbon systems also allows focus to be placed on the catalyst and its role. The model compound 4-(naphthylmethyl)bibenzyl (NBBM) mimics some of the important attributes of coal, e.g., a fused two-ring aromatic connected to other aromatics by short alkyl chains. However, its structure, illustrated in Figure 1, is simple enough to allow for quantitative analysis.

Two studies of the reaction of NBBM have been published. Farcasiu, et al.² reacted NBBM with the hydrogen donor 9,10-dihydrophenanthrene (DHP) thermally and in the presence of a catalytic carbon material. They observed products from thermal fission of each of the bonds labeled in Figure 1, followed by radical capping with DHP derived hydrogen. Reaction with the carbon catalyst increased NBBM conversion and showed, upon subtraction of the thermal background, nearly 100% selectivity to bond A scission. The thermal and catalytic (catalyst precursor $\text{Fe}(\text{CO})_3(\text{PPh}_3)_2$) reactions of NBBM under both hydrogen and nitrogen atmospheres at 420 °C have been examined by Walter et al.³ They classified the main products from reaction of NBBM into three major classes: bond A scission products, bond D scission products, and

hydrogenation products. Walter et al.³ proposed a reaction scheme that consists of the rupture of the thermally weak bond D, followed by bond A cleavage through ipso-substitution of a benzyl radical and subsequent liberation of a methylbenzyl radical. Bond A scission products are naphthyl phenyl methane (from benzyl ipso-substitution), naphthalene, tetralin, methyl benzyl and p-xylene (secondary product from methylbenzyl). Bond D scission products are 4-(naphthylmethyl)toluene and toluene, and hydrogenation products are hydrogenated NBBM species (e.g., 1,2,3,4-tetrahydro NBBM). The stoichiometry for bond A scission was consistent with ipso-substitution by benzyl and H[•] radicals, since the sum of the molar yields of naphthyl phenyl methane, naphthalene and tetralin is equal to the sum of the molar yields of methylbenzyl and p-xylene.

The objective of the present paper is to report on the reaction of NBBM in the presence of a series of substituted iron-carbonyl catalyst precursors at 400°C under a hydrogen atmosphere. We first describe the preparation of the catalytic materials, followed by a description of the reaction system and procedures. Quantitative kinetics are examined through a lumped reaction network. A consistent catalytic reaction mechanism, consisting of the insertion of catalytically bound hydrogen into the naphthalene ring leading to bond A scission and/or hydrogenation, is discussed.

EXPERIMENTAL

Preparation of Catalytic Materials: The reagents for the synthesis of the catalysts, triphenylphosphine (99%, Aldrich), Fe(CO)₅ (99.5%, Alfa Research Chemicals) and Fe₂(CO)₉ (99.7%, Alfa Research Chemicals), were used as received. All solvents were distilled under N₂ over 4 Å molecular sieve to remove oxygen and water, and reactions were performed under an atmosphere of purified nitrogen in Schlenk-type glassware to exclude air and water.

Fe(CO)₄PPh₃ Synthesis: Fe(CO)₄PPh₃ was prepared by a combined photochemical and thermal route from triphenylphosphine (PPh₃) in iron pentacarbonyl (Fe(CO)₅), following the synthesis procedure of Conder and Darensbourg⁴. This preparation procedure, which is selective to the monosubstituted product, is outlined in Figure 2a. Thus, 3 g of PPh₃ (0.011 mole) was added to 28 ml of Fe(CO)₅ (0.208 mole) under a dry N₂ atmosphere. The stirred solution was irradiated with a 100-Watt long-wave UV lamp for 2 hours. The lamp was then turned off and the solution was held at reflux conditions (100°C) for one hour, followed by an additional hour of reflux with the UV lamp turned on. At the end of the reaction sequence, excess Fe(CO)₅ was removed in vacuo. The residue was extracted with 50 ml THF and separated on a neutral alumina chromatography column in air, eluting with 75 ml THF. 50 ml of distilled water was then added and the solution volume reduced under vacuum to precipitate pale yellow crystals that were collected by filtration and purified by recrystallization from heptane. The above procedure gave a 50% yield of Fe(CO)₄PPh₃ (based on PPh₃). The product was identified through melting point comparison, 198-200°C (lit.⁵: 201-203°C) and spectroscopy, IR: ν(CO) (CH₂Cl₂): 2051, 1974, 1939 cm⁻¹ (lit.⁸ ν(CO) (CHCl₃): 2059, 1978, 1938 cm⁻¹).

Fe(CO)₃(PPh₃)₂ Synthesis: Fe(CO)₃(PPh₃)₂ was prepared from Fe(CO)₅ and PPh₃ in refluxing cyclohexanol, following the procedure of Clifford and Mukherjee⁶ outlined in Figure 2b. In this synthesis, 2 ml of Fe(CO)₅ (0.015 mole) and 5 g of PPh₃ (0.018 mole) were added to 100 ml of cyclohexanol. The solution was then refluxed (161°C) for 1 hour under N₂. 100 ml of hexane was added to the reaction solution which was then cooled, giving a yellow precipitate. This relatively straightforward procedure gave a 39% yield (based on Fe(CO)₅) of the disubstituted product, Fe(CO)₃(PPh₃)₂, with a small amount of the monosubstituted derivative, Fe(CO)₄PPh₃, present, which was removed by silica gel chromatography. The product was identified through melting point comparison, 265-285°C (lit.⁸: 272°C) and spectroscopy, IR: ν(CO) (CH₂Cl₂): 1882 cm⁻¹ (lit.⁸: ν(CO) (CHCl₃): 1887 cm⁻¹).

Fe(CO)₂(PPh₃)₂CS₂ Synthesis: Fe(CO)₂(PPh₃)₂CS₂ was prepared from diiron nonacarbonyl (Fe₂(CO)₉) and PPh₃ in refluxing (46°C) carbon disulfide (CS₂), as outlined by

Baird et al.⁷ The route is outlined in Figure 2c. A mixture of 1.5 g of $\text{Fe}_2(\text{CO})_9$ (0.004 mole) and 3 g of PPh_3 (0.011 mole) in 25 ml of CS_2 was refluxed under N_2 for 40 minutes. The solution was cooled, and the rust-red solid, $\text{Fe}(\text{CO})_2(\text{PPh}_3)_2\text{CS}_2$, was precipitated by addition of diethylether (~5-10% yield based on $\text{Fe}_2(\text{CO})_9$). The product was identified through melting point comparison, 133°C (lit.¹⁰: 130-134°C) and spectroscopy, IR: $\nu(\text{CO})$ (CH_2Cl_2): 1990, 1929 cm^{-1} (lit.¹⁰: $\nu(\text{CO})$ (CHCl_3): 1989, 1929 cm^{-1}).

NBBM Reactions: NBBM (TCI Americas), dichloromethane (Fisher Scientific) and all other chemicals (Aldrich Chemical Company) were used as received. The reactions were carried out in 7 cm^3 stainless steel microbatch reactors. The reactant and catalyst precursor were placed in an open 10 x 75 mm glass tube within the reactor to prevent wall interactions. The loadings of NBBM and catalyst precursor were 50 mg and 1.4 wt% by iron, respectively (5 mg for $\text{Fe}(\text{CO})_4\text{PPh}_3$, 8 mg for $\text{Fe}(\text{CO})_3(\text{PPh}_3)_2$, 8.3 mg for $\text{Fe}(\text{CO})_2(\text{PPh}_3)_2\text{CS}_2$), and all reactions took place under 1000 psig (cold) hydrogen pressure. The reactor was pressurized to 1000 psig with hydrogen and then discharged three times prior to heat up. This ensured reaction in the absence of air. The reactor was then plunged into a fluidized sand bath at 400°C and, after the passage of the reaction time, removed from the sandbath for cooling in an ice bath for at least 30 minutes. A known amount of biphenyl was then added to the contents of the glass tube, which was subsequently diluted with dichloromethane. The mixture was then separated in a Hewlett-Packard 5890 Gas Chromatograph with Flame Ionization Detector and a Hewlett-Packard 5890 Gas Chromatograph with a Hewlett-Packard 5970 Mass Selective Detector. Both Gas Chromatographs used Hewlett-Packard Ultra 2 columns (crosslinked 5% Ph Me Silicone) with dimensions 50 m x 0.2 mm and 0.33 mm film thickness.

RESULTS AND DISCUSSION

The reactions of NBBM were studied at 400 °C under 1000 psig (cold) hydrogen pressure in the presence of each of the catalyst precursors ($\text{Fe}(\text{CO})_4\text{PPh}_3$, $\text{Fe}(\text{CO})_3(\text{PPh}_3)_2$, $\text{Fe}(\text{CO})_2(\text{PPh}_3)_2\text{CS}_2$) and in the absence of a catalytic precursor.

The disappearance kinetics shown in Figure 3 reveal that the three catalyst precursors had significant activity above the thermal baseline for the disappearance of NBBM. $\text{Fe}(\text{CO})_4\text{PPh}_3$ led to the highest conversion over most of the reaction times. Conversion in the presence of $\text{Fe}(\text{CO})_2(\text{PPh}_3)_2\text{CS}_2$ was initially lower than in the presence of $\text{Fe}(\text{CO})_3(\text{PPh}_3)_2$, but by 60 minutes the trend had reversed.

Figure 4 is a plot of the yields of the three product classes, i.e., bond A scission, bond D scission and hydrogenation products, versus NBBM conversion for reaction at 400°C in the presence of the three catalyst precursors. The predominate activity for bond A scission and NBBM hydrogenation is clear. Figure 4 shows that, for the catalyst precursor $\text{Fe}(\text{CO})_4\text{PPh}_3$, the rate of appearance of bond A scission products decreases markedly between 120 and 150 minutes. There was very little NBBM left in the reaction mixture at this point (Figure 3); however, there was a significant amount of hydrogenated NBBM (Figure 4). The stoichiometry for bond A scission during reaction with each of the three catalyst precursors at 400 °C was consistent with the results observed by Walter et al.³ and discussed earlier. Ipso-substitution by either benzyl or H^\cdot radicals can account for the observed product distributions.

Figure 5 is a simple reaction network that describes NBBM reaction in terms of the three product lumps: bond A scission products, bond D scission products and NBBM hydrogenation products. The network also includes an "other products" lump, which accounts for products not identified through gas chromatography, e.g., gases and high molecular weight products. Two additional product classes account for secondary reactions to hydrogenated versions of products attributed to bond A and bond D scission.

Quantitative kinetics analysis was accomplished by optimizing network predictions against the experimental data. Table 1 contains the best-fit values of first-order rate constants obtained by parameter estimation using a simplex optimization routine. Model predictions, with the experi-

mental data, for NBBM consumption are shown in Figure 6. The fits are good for reaction thermally and in the presence of $\text{Fe}(\text{CO})_3(\text{PPh}_3)_2$. However, for reaction in the presence of $\text{Fe}(\text{CO})_4\text{PPh}_3$ and $\text{Fe}(\text{CO})_2(\text{PPh}_3)_2\text{CS}_2$ the fits are poor, due to highly non-first order behavior.

The rate constants do provide insight into the reaction mechanisms. The values for the bond D scission constants, k_D , are independent of the presence of the three catalysts. That is, k_D for reaction with any of the catalysts is not significantly different than that during thermal reaction. This suggests that bond D scission is purely thermal and is unaffected by the presence of a catalyst. Similarly, the values for the bond A scission constants, k_A , are similar for reaction with each of the three catalysts and quite different than that for thermal reaction. This suggests that a single mechanism is responsible for the bond A scission in the presence of the three catalyst precursors. In addition, the values of the hydrogenation constants, k_H , are consistent with the higher hydrogenation activity observed for $\text{Fe}(\text{CO})_4\text{PPh}_3$ catalyst than for the other two shown in Figure 4. Also, the slower scission of bond A in hydrogenated NBBM relative to that for bond A scission of NBBM is reflected in the relationship $k_{HA} < k_A$ for all three catalyst precursors. Finally, all three catalyst precursors showed higher activity for hydrogenation of naphthalene (k_{AH}) than for hydrogenation of the substituted naphthalene (k_H).

Mechanistic insights derive from the known activity of reduced iron as an effective hydrogenation catalyst. The iron likely dissociates hydrogen into atoms that can, in turn, add to the naphthyl ring. When a hydrogen inserts at the ipso position, a thermochemically favorable β -scission pathway affords naphthalene and a methylbenzyl radical. This proposed mechanism is also consistent with the lack of bond A scission of hydrogenated NBBM. The destruction of the electron rich naphthalene system both decreases the molecule's ability to interact with the catalyst and removes the electronic topology required for ipso-substitution.

CONCLUSIONS

The catalytic chemistry of NBBM at 400°C under a hydrogen atmosphere in the presence of the series of iron-carbonyl based catalyst precursors $\text{Fe}(\text{CO})_4\text{PPh}_3$, $\text{Fe}(\text{CO})_3(\text{PPh}_3)_2$ and $\text{Fe}(\text{CO})_2(\text{PPh}_3)_2\text{CS}_2$ was examined. The three catalyst precursors showed significant activity for the disappearance of NBBM above the thermal baseline. Two of the main product classes were "bond A scission" and "NBBM hydrogenation". Quantitative network analysis examined the kinetics for each reaction family among the catalyst precursors. This analysis indicated that: bond D scission was purely thermal and unaffected by the presence of the catalyst precursors; bond A rate constants were similar for reaction in the presence of all three catalyst precursors and different from that for thermal reaction; and the hydrogenation rate constant was higher for $\text{Fe}(\text{CO})_4\text{PPh}_3$ than for the other two catalyst precursors. A consistent reaction mechanism involves catalytic dissociation of H_2 into hydrogen atoms, which are, in turn, inserted into the naphthalene system of NBBM; the naphthalene site at which the hydrogen atom is inserted determines the outcome of bond A scission or hydrogenation. The slower rate of bond A scission observed by the hydrogenated NBBM species can be qualitatively explained with decreased catalyst interaction and removal of ipso-substitution electronic topology.

ACKNOWLEDGMENT

We would like to thank Dr. William H. Calkins, Dr. G. Alex Mills and Dr. Malvina Farcasiu for discussions in the area of coal chemistry and coal catalysis, and Dennis Kalaygian for his help in performing some of the NBBM reaction experiments. This work was supported by the United States Department of Energy Grant DE-AC22-90PC90050.

¹ Larsen, John W., Wernett, Patrick, "Pore Structure of Illinois No. 6 Coal", *Energy & Fuels*, **2** (5), 719-720, 1988

² Farcasiu, Malvina, Smith, Charlene, "Modeling Coal Liquefaction, 1. Decomposition of 4-(1-Naphthylmethyl)benzyl Catalyzed by Carbon Black", *Energy & Fuels*, **5**(1), 83-87, 1991

³ Walter, Timothy D., Casey, Stephen M., Klein, Michael T., Foley, Henry C., "Reaction of 4-(naphthylmethyl)biphenyl Thermally and in the Presence of $\text{Fe}(\text{CO})_2(\text{PPh}_3)_2$ ", submitted for publication, Presented at DOE Liquefaction Contractors' Meeting, Pittsburgh, PA Sept. 22-24, 1992

⁴ Conder, H.L., and Darensbourg, M. York, "The Synthesis of Group V Substituted Derivatives of Iron Pentacarbonyl in High Yield", *J. Organomet. Chem.*, 1974, **67**, 93-97.

⁵ Cotton, F.A. and Parish, R.V., "The Stereochemistry of Five-coordinate Compounds. Part I. Infrared Spectra of Some Iron(0) Compounds", *J. Chem. Soc.*, 1960, 1440-1446.

⁶ Clifford, A.F., and Mukherjee, A.K., "Iron Carbonyl Complexes of Triphenylphosphine, Triphenylarsine, and Triphenylstibine", *Inorg. Chem.*, 1963, **2**, No. 1, 151-153.

⁷ Baird, M.C., Hartwell, jun., G., and Wilkinson, G., "Carbon Disulphide Complexes of Vanadium, Iron, Cobalt, Ruthenium, and Iridium; the Preparation of trans-Bis(triphenylphosphine)thiocarbonylhalogeno-rhodium(I) and -rhodium(III) Complexes", *J. Chem. Soc. (A)*, 1967, 2037-2040.

	$(\text{k}_1 / \text{s}^{-1}) \times 10^5$			
	Thermal	$\text{Fe}(\text{CO})_4\text{PPh}_3$	$\text{Fe}(\text{CO})_3(\text{PPh}_3)_2$	$\text{Fe}(\text{CO})_2(\text{PPh}_3)_2\text{CS}_2$
k_A	0.455	4.32	3.00	4.19
k_H	0.035	15.8	5.59	6.59
k_D	0.457	0.366	0.454	0.363
k_{AH}	4.92	42.4	18.2	17.8
k_{DH}	1.83	4.44	6.36	8.87
k_{HA}	0.112	1.72	1.33	0.549
k_{HD}	0.031	0.505	0	0
k_O	1.11	5.91	2.78	2.99

Table1: Regressed values for the first-order rate constants for the reaction network of Figure 5.

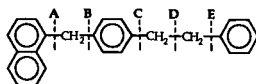
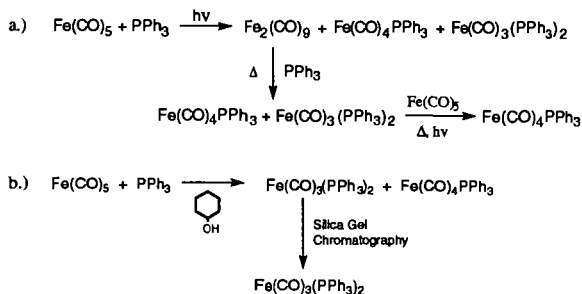


Figure 1: Model compound, 4-(naphthylmethyl)biphenyl.



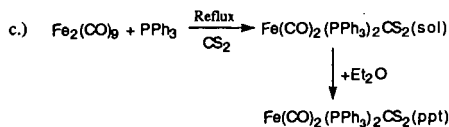


Figure 2: Synthesis routes for: a) $\text{Fe}(\text{CO})_4\text{PPh}_3$; b) $\text{Fe}(\text{CO})_3(\text{PPh}_3)_2$; $\text{Fe}(\text{CO})_2(\text{PPh}_3)_2\text{CS}_2$.

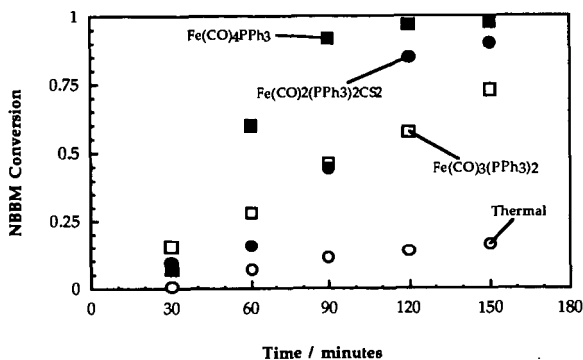


Figure 3: Kinetics of NBBM disappearance at 400°C under 1000 psig H_2 (cold) in the presence of iron carbonyl based catalyst precursors.

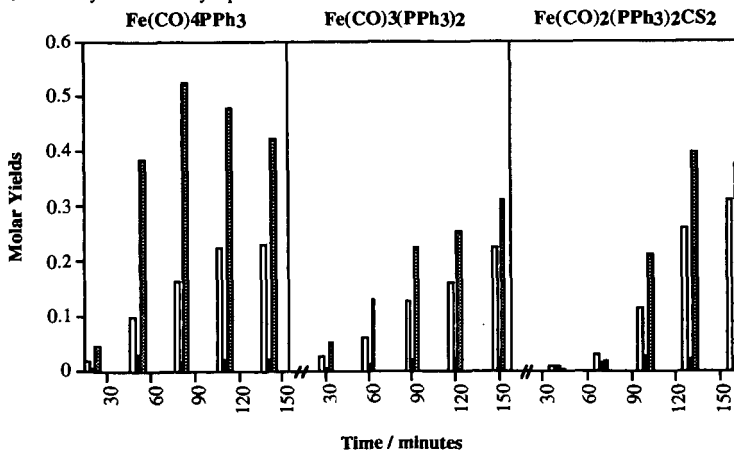


Figure 4: Molar yields of bond A scission, bond D scission and NBBM hydrogenation products classes upon reaction of NBBM at 400°C under 1000 psig H_2 (cold) in the presence of iron carbonyl based catalyst precursors. □ Bond A Scission Products; ■ Bond D Scission Products; ▨ Hydrogenation Products.

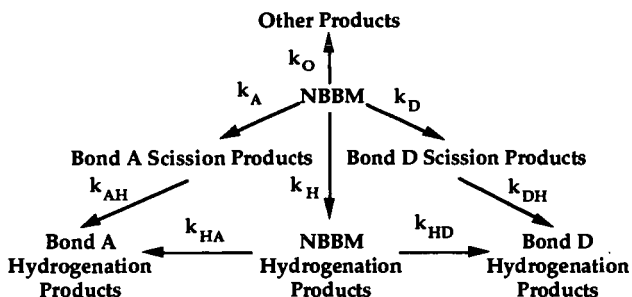


Figure 5: Lumped network for the reaction of NBBM at 400°C under 1000 psig H₂ (cold) in the presence of iron carbonyl based catalyst precursors.

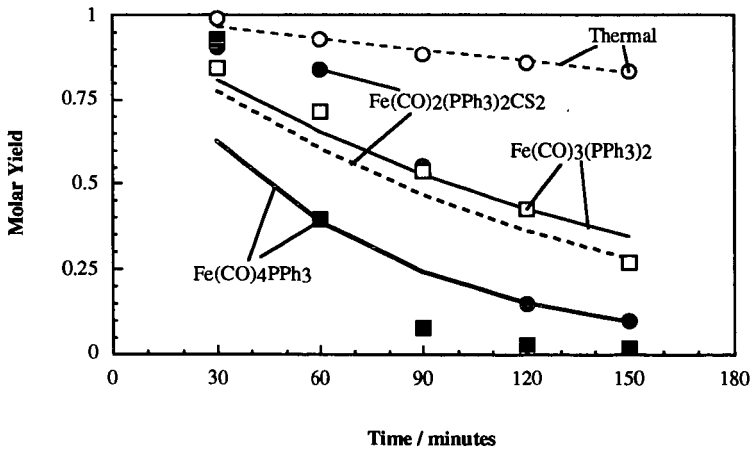


Figure 6: Model fits for the lumped network describing the reaction of NBBM at 400°C under 1000 psig H₂ (cold) in the presence of iron carbonyl based catalyst precursors. The lines are the predicted curves and the points are the experimentally measured values.

**Complex Iron Catalytic Systems: Relative Catalytic Activity
of Various Components.**

Malvina Farcasiu, Patricia A. Eldredge and Steven C. Petrosius

U.S. Department of Energy
Pittsburgh Energy Technology Center
P.O. Box 10940, Pittsburgh PA 15236

Key words: catalytic hydrocracking, iron-sulfur catalysts, active phase.

ABSTRACT

Fine particle (6-8nm) iron-sulfur systems with complex chemical compositions are formed when a 3 nm iron oxide is heated with sulfur in the presence of 9,10-dihydrophenanthrene for 1 hour. These systems form small-particle pyrrhotite when heated at 320°C. The fine particle pyrrhotites are very active hydrocracking catalysts, but agglomerate rapidly during reaction at 320°C.

INTRODUCTION

The use of iron-based catalysts in reactions of interest for direct coal liquefaction usually involves the addition of iron compounds to the reaction mixture and the in-situ activation of the iron compounds to form iron catalysts. The composition of active iron-based catalysts has been a subject of considerable interest and several reviews have been published on the subject (1,2). It was reported that the hydrocracking of monoaromatic model compounds at temperatures of 425-435°C is catalyzed by iron-sulfur systems in the presence of hydrogen sulfide (2). The catalytic activity was tentatively explained by an interaction of pyrite with pyrrhotite and hydrogen sulfide.

We have studied the activity of some iron-sulfur catalytic systems formed in the reaction of fine-particle iron oxides with elemental sulfur and a hydrogen donor, 9,10-dihydrophenanthrene (9,10-DHP), at low temperature. In this paper we will discuss the systems formed when the above compounds are heated at low temperatures (200 - 320°C). We have found that the iron-sulfur systems formed under these conditions are very active in low temperature, selective hydrocracking of C_{ar}-C_{aliph} bonds, when the aromatic carbon is a part of a condensed polycyclic aromatic hydrocarbon. The composition of the iron-sulfur systems and the variation of their compositions with time under various reaction conditions have been studied by a variety of methods. We report

here our findings concerning the catalytically active components in the above described iron-sulfur system.

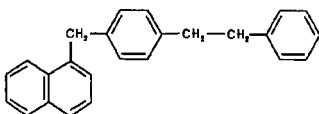
EXPERIMENTAL

General. Reagent grade chemicals and HPLC grade solvents were used as purchased unless stated otherwise. Methylene chloride was dried over 4 Å molecular sieves. Ferrihydrite ($5\text{Fe}_2\text{O}_3 \cdot 9\text{H}_2\text{O}$), obtained from Mach I, Inc., King of Prussia, Pennsylvania, was vacuum dried for ca. 3 hours at 150 °C, then stored in a desiccator. The particle size reported by the vendor (3-5 nm) was confirmed by microscopic analysis and is consistent with the surface area determination by the BET method. Compound I was available from our previous work (3).

The reactions were conducted in sealed 7mm o.d. heavy walled glass tubes (Corning Glass) in a Lindberg Type 59344 muffle furnace equipped with a thermocouple.

Chromatographic analyses were conducted on a Hewlett-Packard Model 5890 Series II Gas Chromatograph equipped with a split-vent injector and connected to an HP 3396A integrator, on a J&W 30 m x 0.248 mm fused silica capillary column coated with 0.25 μm silicone SE-52, with a head pressure of 20 psi (136 KPa). The column temperature was increased from 80°C to 310°C at a rate of 8°C/min. Identification of the components was described in a previous publication (3).

Catalyst Preparation and Activity Measurement. In a typical experiment, ferrihydrite (2.5 mg) dried as indicated above, sulfur (2.5 mg), and 9,10-DHP (100 mg) were loaded into the glass tube which was sealed without excluding the air. The length of the sealed tube was ca. 14 cm. The tube was heated at the desired temperature for the duration indicated below, then it was cooled and stored at room temperature until use. For catalyst testing, the tube was cracked open (CAUTION: pressure buildup in the tube occurs, particularly for experiments at higher temperatures), 25 mg of the reactant, 4-(1-naphthylmethyl)bibenzyl (I), was added and the tube was resealed and heated as indicated



below. In the alternative procedure, compound I was added together with the catalyst precursors such that catalyst preparation and reaction of I were conducted in one operation. For the analysis of

products, the tube was cooled to room temperature and carefully opened, the organic materials were dissolved in the minimum amount of methylene chloride possible and filtered through a layer of anhydrous MgSO_4 (ca. 0.3 g) supported by a glass wool plug in a micropipette. The tube was rinsed twice with methylene chloride (ca. 0.5 mL each time) and the washings were filtered through the same microcolumn for drying. The combined solution was concentrated to ca. 1 mL and analyzed by GLC (0.5 μL of sample was used for each injection).

Catalyst Characterization. The particle size, chemical composition, and the crystallographic properties of the iron species formed under various experimental conditions were determined as described by Eldredge et al.(4), using XRD and Moessbauer spectroscopy. The surface area was determined by the BET method (5) from the adsorption isotherms for N_2 at 77K. The samples were first outgassed for 18 hr at 95°C and less than 10^3 torr. A Coulter Omnisorp 100CX gas sorption analyzer operated in the fixed-dose, static-flow volumetric mode was used to measure the adsorption isotherms. Equilibration of the sample with a nitrogen dose was defined as five consecutive readings with a variance of less than 0.1 torr over a 3 second interval. A value of 0.162 nm^2 was used for the cross-sectional area of nitrogen.

RESULTS AND DISCUSSION

The catalyst prepared in-situ from ferric oxide (20-80 nm) and sulfur in the presence of 9,10-DHP and reported previously (6) was found active in hydrocracking reactions of compound I at temperatures of 420-430°C. In the present study, the reactions were performed at temperature and conditions where no thermal reaction of I occurs (3). In work reported here, we have used an oxide with smaller particles (3-5 nm) as the catalyst precursor. Our goal was to prepare an iron-sulfur catalyst in an initial step, and then add the substrate I and perform the hydrocracking reaction. The temperature was varied independently in the two steps (between 200°C and 320°C for the first step and between 200°C and 400°C for the second step) and each step was normally conducted for 1 hour. Alternatively, the two steps were combined by adding the substrate from the beginning and thus synthesizing the catalyst in-situ. The conversion of I, defined as the selective cleavage of the bond adjacent to the naphthalene ring, is presented in Table 1 for both of these approaches. It can be seen that the catalyst is active even at temperatures as low as 250°C. Moreover, conversion of I reaches a maximum value of 92% in one hour at 350°C (Table 1)

The data in Table 1 also show that reaction of I at any temperature between 250 and 400°C gives the same conversion with the catalyst generated in-situ or with the material pre-synthesized at 200°C. Synthesis of the catalyst in a prior step at higher temperatures gave less active catalytic systems.

Under our experimental conditions, specifically with the reactant dissolved in 9,10-DHP, there is likely no mass transfer limitation and the rate of formation of the active phase by the

reaction of iron oxide with sulfur (or more likely with the hydrogen sulfide formed from S and the H-donor) is faster than the hydrocracking reaction. Such favorable conditions might not be available if the catalyst were generated in a very complex heterogenous medium with large excess of solids, as is the case in coal liquefaction. Therefore, preparation of active, small particle catalysts, prior to the actual coal liquefaction, is desirable.

The structural study of this Fe-S material formed after pretreatment of 3-5 nm particles of ferrihydrite for 1 hour at 200°C indicates the presence of at least four distinct components: pyrrhotite, magnetite, unreacted ferrihydrite (or hematite), and a new iron sulfide phase identified as marcasite with pyrite stacking faults (4). The composition, as determined by Moessbauer spectroscopy, is reported to be (7): 15% pyrrhotite, 19% unreacted ferrihydrite, 29% magnetite, and 37% for the new iron sulfide phase. The particle size of the pyrrhotite component in this material was in the range of 6.5-8 nm (XRD) and its calculated surface area was 150-182 m²/g. The direct surface area determination for all the components gave a surface area of 180 m²/g. The marcasite/pyrite phase is unstable at 200°C and is converted to pyrrhotite upon longer heating at that temperature. Pyrrhotite is also formed at the expense of the new phase when catalyst synthesis is conducted at higher temperature. In both cases, larger particles are obtained. When catalyst preparation was conducted at 320°C, only pyrrhotite was observed even at a short reaction time of 20 minutes. The particle size of the pyrrhotite obtained under the latter conditions was ~30 nm, with a corresponding calculated surface area of ~40 m²/g. Pretreatment at 200°C, followed by treatment for 10 minutes at 320°C, or direct pretreatment for 10 minutes at 320 °C gives pyrrhotite with particle size of 22-25 nm (corresponding surface area of 54-48m²/g). After pretreatment of 1 hour at 320°C, the particle size of the pyrrhotite was in the range of 38-50 nm (XRD) and a surface area of ~24 m²/g was calculated.

The catalytic activity of the iron-sulfur system formed at 200°C may be due to one, some, or all of the components present; i.e., to pyrrhotite, the newly identified iron sulfide phase, magnetite, or to the unreacted ferrihydrite. The ferrihydrite used alone in tests with I in the presence of 9,10-DHP was found to be catalytically inactive. For identification of the active phase in this system, we studied the conversion of compound I at 320°C as a function of time in the presence of the iron-sulfur system presynthesized at 200°C. The results are given in Table 2. Based on the conversion at 40 minutes with pyrrhotite of 24 m²/g initial surface area, a specific catalytic activity for pyrrhotite of 0.39 nmoles I/(m²hour) is calculated. X-ray diffraction data indicate that pyrrhotite is the primary material present after 20 minutes at 320°C. Assuming the only catalytically active phase present even at short reaction time is pyrrhotite, then for the 45% conversion of I in the first 20 minutes of the reaction, an average surface area of 108 m²/g can be calculated for this interval using the specific activity mentioned above. This value compares well with the observed decrease in the surface area during the first 20 minutes of reaction from ~180 m²/g

to $\sim 41 \text{ m}^2/\text{g}$ (a calculated average would be $110 \text{ m}^2/\text{g}$). Using this result along with the observation that pyrrhotite is by far the major component in the system leads to the conclusion that pyrrhotite is most likely the catalytically active phase.

The possible catalytic activity of magnetite (a major component after pretreatment of the mixture of ferrihydrite and sulfur in the presence of 9,10-DHP at 200°C for 1 hour) was studied using samples of genuine magnetite of known particle sizes (8). However, based on the observed conversion to pyrrhotite after 20 minutes at 320°C , it is unlikely that magnetite makes any important contribution to the activity under the reaction conditions reported in Table 2. The observed conversions after pretreatment at various temperatures can be explained by pyrrhotite as the catalytically active phase and by the variation of its particle size (surface area) as a function of the experimental conditions. Consequently, our present data indicate no measurable catalytic activity for the new form of pyrite-marcasite identified when the iron-sulfur system is preformed at 200°C , as described above. However, the stability at room temperature of the iron-sulfur system formed after pretreatment for 1 hour at 200°C without loss of the catalytic activity (Table 3) may be due to the fact that this complex system prevents the agglomeration of the particles.

Data by Cugini et al. (9) show that when highly dispersed FeOOH is precipitated on coal and the coal is pretreated at 275°C in presence of a sulfur compound, an active catalyst for coal liquefaction can be formed. It is likely that this catalyst is highly dispersed pyrrhotite and that coal prevents its agglomeration. However, in the absence of sulfur, other iron compounds are stable and can act as catalysts. When a low sulfur bituminous coal is liquefied in the presence of magnetite, a significant catalytic activity is observed and magnetite is observed as such at the end of reaction (8).

CONCLUSIONS

We have found that pretreatment of fine particle size (30 nm) iron oxide with sulfur in the presence of 9,10-DHP, at 200°C for one hour gives a high surface area mixture of magnetite, pyrrhotite, and a newly identified phase of marcasite-pyrite (4). We studied this system for hydrocracking reactions of compound I at various temperatures. The iron-sulfur mixture transforms at 320°C (the temperature at which we report kinetic data) into pyrrhotite. The surface area of pyrrhotite varies with the reaction time and the catalytic activity can be correlated to the surface area variation. The observed catalytic activity in the hydrocracking reaction of I is attributed under these conditions to pyrrhotite.

ACKNOWLEDGEMENTS

The authors gratefully acknowledge the contribution of Dr. S. Pollack, Dr. N. Johnson and Mrs. E. Frommel from PETC for their assistance with XRD analyses and helpful discussions. Technical

discussions with prof. I. Wender, Dr. B.D. Blaustein and Dr. R.P. Warzinski are gratefully acknowledged. This work was supported in part (PAE and SCP) by appointments to the Department of Energy Fossil Fuels Energy Postgraduate Research Training Program administered by Oak Ridge Institute for Science and Education.

DISCLAIMER

Reference in the paper to any specific commercial product, process or service is to facilitate understanding and does not necessarily imply its endorsement or favoring by the United States Department of Energy.

REFERENCES

1. Trawhella, M.J.; Grint, A. Fuel, 1987, 66, 1315 and references therein.
2. Narain, N.K.; Cillo, D.L.; Stiegel, G.J.; Tisher, R.E. Coal Science and Chemistry, A. Volborth editor, Elsevier Science Publishers B.V., Amsterdam, 1987, pp 111-149 and the references therein.
3. Farcasiu, M.; Smith, C.M. Energy & Fuels, 1991, 5, 83.
4. Eldredge, P.A.; Frommell, E.A.; Huggins, F.E.; Pollack, S.P., 1992, unpublished work.
5. Brunauer, S.; Emmett, P.H.; Teller, E. J. Am. Chem. Soc., 1938, 60, 309.
6. Farcasiu, M.; Smith, C.M.; Pradhan, V.R.; Wender, I. Fuel Processing Technology, 1991, 29, 199.
7. Huffman, G.P.; Huggins, F.E., personal communication.
8. Farcasiu, M.; Petrosius, S.C.; Warzinski, R.P., unpublished work.
9. Cugini, A.V.; Utz, B.R; Krastman, D.; Hickey, R.F. Prepr. Pap.- Am. Chem. Soc. Div. Fuel Chem. 1991, 36, 91.

Table 1. Catalytic Conversion of I at Various Temperatures in the Presence of Iron-Sulfur Catalysts.

Conditions: 25 mg I, ~100 mg 9,10 DHP, 10 wt% (based on I) ferrihydrite, 10 wt% (based on I) sulfur, 1h reaction time.

Reaction Temperature °C	Conversion of I, %			
	no catalyst pretreatment	pretreatment 1h at		
		200°C	250°C	320°C
200	0	0	0	0
250	10	9	0	0
275	31	32	10	-
300	52	54	30	10
320	79	78	48	17
350	92	92	66	38
400	94	93	87	40

Table 2. Catalytic Conversion of I at 320°C as Function of Time.

Time h	Catalytic Conversion % in presence of	
	Pyrrhotite* ~24m ² /g	Catalyst from 200°C, 1h pretreatment
0.33	~ 12	45
0.5	13	57
0.66	20	65
1	17	79

* Pyrrhotite obtained after pretreatment for 1h at 320°C.

Table 3. Stability of the Iron-Sulfur System Preformed at 200 °C Reaction of I at 320°C, 1 hour.

Storage Time days	Conversion of I %
0	79
1	79
3	73

MOLECULAR ORBITAL CALCULATIONS FOR IRON CATALYSTS

Harriet F. Ades, Audrey L. Companion, and K.R. Subbaswamy
Departments of Physics and Chemistry
University of Kentucky, Lexington, KY 40506-0055

Keywords: Iron Catalysts, Quantum Chemistry, Clusters

One of the primary questions facing scientists working in the area of direct coal liquefaction (DCL) is the state of the iron in iron-based catalysts. While much work has been done on iron-based DCL catalysts, the mechanism of catalysis is poorly understood. In order to elucidate the possible catalytic action, we have begun modeling various surfaces of FeS and $\text{Fe}_{(1-x)}\text{S}_y$ clusters with the ASED-MO method of Anderson. We have studied the adsorption of toluene and 1-methylnaphthalene at various sites on FeS and related defect clusters and have calculated bond breaking energies of the aromatic-aliphatic linkage. One explanation of the catalytic activity of the FeS is donation of electrons to the iron surface by the adsorbate, followed by a subsequent decrease in the bond breaking energies as compared to nonchemisorbed toluene or 1-methylnaphthalene.

A. Introduction

The development of effective and economical catalysts is the key to making direct coal liquefaction a commercially viable goal. To this end, there has been a great deal of interest in sulfided iron catalysts for coal liquefaction. Several facts are known from experiments: the presence of sulfur increases the liquefaction conversion;¹ molybdenum is a 'more active catalyst' for liquefaction than iron;² molybdenum produces a more highly hydrogenated product; and the addition of molybdenum to the iron sulfided catalysts greatly increases the activity of the iron catalyst.¹ However, the question of the state of the iron in the iron-based catalysts is still unanswered. For instance, in experiments starting with iron oxide as the catalyst it is still not known whether the iron oxide undergoes a phase transition directly to Fe_xS_y phases or it transforms to metallic iron first and then goes to form Fe_xS_y .³ We address such questions through quantum chemical modeling calculations.

Two methods, both based on the EHMO method of Hoffmann,⁴ are particularly suited for these investigations. The first, a band structure tight binding EHMO approach, developed by Whangbo,⁵ has already been successfully employed by Zonneville, *et al.*⁶ in explaining thiophene desulfurization on MoS_2 and the formation of negatively charged ions in the scattering of oxygen from silver. This method is well suited for investigating bulk and semi-infinite surface properties of the catalyst systems.

The second, the ASED-MO method developed by A.B. Anderson,⁷ has been used by us in the study of the possible cleavage mechanisms of model compounds of interest to investigators in the field.⁸⁻¹¹ Anderson also has used the method to study ethylene hydrogenation mechanisms on Pt surfaces and ethylene and acetylene absorption on MoS_2 clusters.¹² In this method one models a surface by a small number of atoms (i.e., as the surface of a cluster of atoms), and is ideal for the study of the small ultrafine particle catalysts. One can thus

address whether the departure from bulk properties when the catalyst size approaches 10nm is the cause of catalytic activity.

Our goal is to investigate the active sites in both nano-size and large particles of iron-based catalysts by quantum chemical methods. Initially the adsorption of small organic molecules such as ethylene and toluene on various sites on FeS, Fe₇S₈, other defect structures, and pure Fe surfaces will be investigated in order to try to determine the differences in adsorptive and catalytic activity as one progresses from pure iron to the defect pyrrhotite structure. As a prelude to these complex studies, we have begun to model these interactions with cluster studies using the ASED-MO method of Anderson.⁷

B. Method Used

The ASED-MO method is an attempt to improve the binding energy curve calculation in EHMO theory. There are two significant modifications. The first one is in the Hamiltonian matrix. In the ASED-MO method, as in the EHMO method, the molecular orbitals are expanded in terms of Slater type orbitals for the valence electrons. The eigenenergies, ϵ_j , and the expansion coefficients are obtained from a solution of the secular equation,

$$|H_{ij} - \epsilon_j S_{ij}| = 0 \quad (1)$$

The Hamiltonian matrix H in ASED-MO is defined by

$$H_{ii} = -VSIE, \quad (2)$$

$$H_{ij} = \frac{K}{2}(H_{ii} + H_{jj})S_{ij} \exp(-\delta R_{ij}). \quad (3)$$

The S_{ij} 's are overlap integrals and are calculated explicitly with Slater-type orbitals (STO). The valence state ionization energies (VSIE) and the exponents in the STO's are frequently adjusted slightly from experimental or theoretical norms in order to give numbers that are in closer agreement with experiment.¹³ Note that the off-diagonal matrix elements in (3) are different from the usual EHMO form of the Wolfsberg-Helmholz expression by the inclusion of the exponential factor. The constant, K , is taken to be 2.25 in the ASED-MO version, and the exponent δ is 0.13au⁻¹. The R_{ij} 's are the distances between the various atom centers in the molecule. The practical effect of the exponential factor is to produce a sharper increase in the potential curve between any two atoms than the standard standard EHMO methods.

The second modification of EHMO in the ASED-MO method is the inclusion of specific pairwise repulsion terms, derived from the consideration of the Hellman-Feynman force theorem.⁷ Nuclear repulsion terms, attenuated by nuclear attraction integrals, are included in each pairwise repulsion term. The attraction terms are computed with classical formulae, approximating the density due to p and d electrons by spherical distributions. Inclusion of the two modifications of Anderson significantly improves the validity of EHMO calculations.

C. Results and Discussion

The first cluster we investigated is shown in Figure 1 and consists of 19 Fe atoms in the top layer, 12 sulfur atoms in the second layer and 19 iron atoms in the third layer. This particular cluster was chosen because of its simplicity, and more realistic surfaces will

be studied subsequently. The interatomic distances were chosen to correspond to those in the idealized pyrrhotite structure.¹⁴ The nearest neighbor distance between iron atoms in the same layer is 3.43 Å but 2.84 Å between layers. The Fe-S distance is 2.44 Å. This is to be compared with the nearest neighbor distance in bcc pure iron of 2.48 Å. The inner iron atoms of the cluster exhibit a charge of about +0.6 |e|. While this cluster does not have the overall stoichiometry of FeS, it is representative of the correct stoichiometry in the immediate vicinity of the adsorption sites studied.

We started by studying the adsorption of a hydrogen molecule on this cluster. The hydrogen molecule was allowed to approach the top layer of the surface perpendicularly in several different sites—i.e. head-on, bridge, and interstitial (over the exposed sulfur atom in the second layer) sites. These positions are labeled A, B, and C, respectively, in the second panel of Figure 1. The iron pyrrhotite structure was modeled by removing an iron atom from the top layer, thereby creating a vacancy in this layer. The most stable positions for the hydrogen molecule at its ASED minimum energy distance were found. In several cases, once this position was found, the hydrogen atom closest to the surface was fixed and the position of the outermost hydrogen optimized with the grid search option of the ASED program. The binding energy of the hydrogen molecule to the surface was of the order of 0.04-0.07 eV, in other words, a physisorption process is occurring. However, in the presence of the vacancy the physisorption energies slightly decrease, indicating an inhibitory effect as the iron pyrrhotite structure is formed. We next investigated the adsorption of a simple organic molecule, ethylene. The ethylene molecule, at its ASED minimum energy configuration, was brought up parallel to the surface of the cluster. In this manner, the p_z orbitals of the carbon atoms can interact with the d orbitals of iron. The ethylene molecule was allowed to approach with one carbon atom fixed directly above an iron atom and the other carbon atom along the x axis. Once the minimum energy distance above the surface of the molecule was found, the CH_2 fragment not above the iron was allowed to relax until the energy of that fragment was minimized. For each of the sites studied, the binding energy of ethylene to the surface was found to be about 1 eV—i.e., a chemisorption process is occurring. There was almost no difference in binding energies whether the adsorption site was the central iron atom or one removed from the central atom. However, when a vacancy was created, the binding energy of ethylene over the vacancy site (with the sulfur layer underneath) decreased to about 0.25 eV, even after considerable relaxation of the whole ethylene molecule.

In order to compare the effect of the sulfur layer, the second layer was changed to iron (i.e., a pure iron cluster) and the same procedure followed. The adsorption in the absence of the vacancy was the same as for the iron-sulfur cluster. However, in the presence of the vacancy the chemisorption energies did not decrease as much as in the presence of a sulfur layer. Therefore, the presence of sulfur appears to have an inhibitory effect on the chemisorption ability of the cluster surface.

We next studied the adsorption of toluene and 1-methylnaphthalene on the FeS cluster. A typical geometry studied is shown in Figure 2. The ring system of toluene was kept fixed at experimental distances and kept planar. The height of the toluene molecule above the surface and bond distances, angles, dihedral angles of the ring- CH_3 group were optimized coarsely in this preliminary study. The binding of toluene to an iron atom of the surface is about 2.5 eV and of 1-methylnaphthalene about 5 eV. We observe a transfer of charge from the ring systems to the cluster with a resultant decrease in the ring- CH_3 bond breaking energy as compared to unadsorbed toluene and 1-methylnaphthalene: from 4.25 to 2.8 eV for toluene and from 4.18 to 2.6 eV for 1-methylnaphthalene (the geometry of the adsorbed molecules has

not yet been fully optimized, and so the energies are still approximate). Our initial results lead to the conclusion that the compounds are strongly chemisorbed on the catalyst surface, with a resultant transfer of charge from the molecule to the catalyst, leading to a decrease in bond breaking energies. This appears to be similar to the mechanism proposed by Farcasiu, *et al.*¹⁵ in the context of the catalytic decomposition of 4-(1-naphthylmethyl)biphenyl in the presence of carbon black. We are now in the process of doing more rigorous geometry optimizations for the cases considered above and studying other adsorption sites, the effect of iron vacancies, and modeling other surfaces which have sulfur exposed.

D. Acknowledgement

This research was supported by USDOE contract DE-FC22-90PC90029 with the Consortium for Fossil Fuel Liquefaction Science and the University of Kentucky Center for Computational Sciences.

References

1. Pradhan, V.R.; Herrick, D.E.; Tierney, J.W.; Wender, I. *Energy Fuels* **1991**, *5*, 712.
2. Derbyshire, F.; Hager, T.; *Prepr., Div. Fuel Chem., Am. Chem. Soc.* **1992**, *37(1)*, 312.
3. Srinivasan, R.; Keogh, R.A.; Davis, B.H. *Prepr., Div. Fuel Chem., Am. Chem. Soc.* **1992**, *37*, 1265.
4. Hoffmann, R.; *J. Chem. Phys.* **1963**, *39*, 1397.
5. Whangbo, M.-H; Hoffmann, R.; *J. Am. Chem. Soc.* **1978**, *100*, 6093.
6. Zonneville, M.C.; Hoffmann, R.; Hoek, P.J. van den; Santen, R.A. van; *Surf. Sci.* **1989**, *223*, 233 and Zonneville, M.C.; Hoffmann, R.; Harris, S.; *Surf. Sci.* **1988**, *199*, 320.
7. Anderson, A.B.; *J. Chem. Phys.* **1974**, *60*, 2477, (1974).
8. Ades, H. F.; Companion, A. L.; Subbaswamy, K. R. *J. Phys. Chem.* **1991**, *95*, 2226.
9. Ades, H. F.; Companion, A. L.; Subbaswamy, K. R. *Prepr., Div. Fuel Chem., Am. Chem. Soc.* **1991**, *36*, 420.
10. Ades, H. F.; Companion, A. L.; Subbaswamy, K. R. *J. Phys. Chem.* **1991**, *95*, 6502.
11. Ades, H. F.; Companion, A. L.; Subbaswamy, K. R. (to be published).
12. Yu, J.; Anderson, A.B.; *J. Mol. Catal.* **1990**, *62*, 223 and Anderson, A.B.; and Choe, S.J.; *J. Phys. Chem.* **1989**, *93* 6145.
13. Howell, J.; Rossi, A.; Wallace, D.; Haraki, K.; Hoffmann, R. *Quantum Chemistry Program Exchange No. 344* (Indiana University, Bloomington).
14. Fleet, M.E.; *Acta Cryst.* **1971**, *B27*, 1864.
15. Farcasiu, M.; Smith, C.; *Energy Fuels* **1991**, *5*, 83.

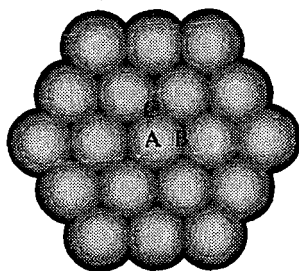
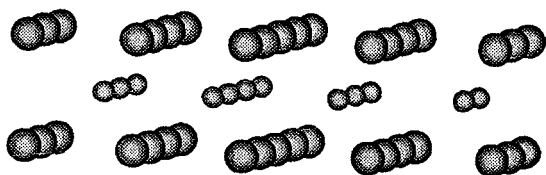


Fig. (1) Top Panel: FeS Cluster
Bottom Panel: Adsorption site labels

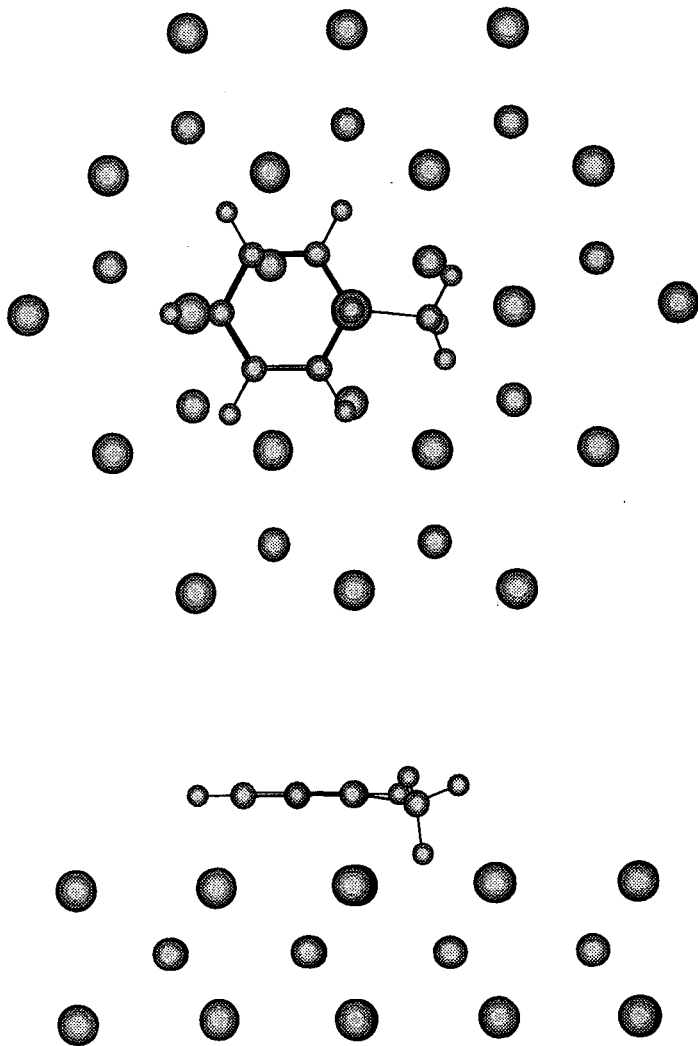


Fig. (2) Chemisorption of toluene on FeS cluster: top and side views

RESULTS OF CATALYST TESTING USING IRON-BASED CATALYSTS

John C. Linehan, John G. Darab, and Dean W. Matson
Pacific Northwest Laboratory¹
P.O. Box 999, Richland, WA 99352.

Keywords: Iron catalysts, Coal liquefaction, Model compounds

ABSTRACT

New bulk and ultrafine iron-based coal liquefaction catalysts have been tested using coal substrates and a model compound. The results of these tests will be presented with emphasis on differences between bulk and ultrafine catalysts. The effects of catalyst size, surface area, and structure on both the model compound reactions and the coal liquefaction reactions will be compared. Special emphasis will be placed upon identifying the best catalyst precursor for optimizing THF soluble yields from coal experiments. In addition, results from different micro-reactors for coal liquefaction will be compared.

INTRODUCTION

As coal liquefaction catalysts, iron-based products are generally inferior to the more expensive molybdenum, cobalt, or nickel-based materials. However, the lower costs of production and recovery (or in the case of some iron catalysts, non-recovery) give the iron-based materials a potential economic advantage over the more efficient precious and semi-precious metal catalysts for this application. Recent research has shown that a number of different iron-containing materials can be successfully utilized as coal liquefaction catalysts or as catalyst precursors.²⁻⁶

Pyrrhotite ($Fe_{1-x}S$) or a similar iron-sulfide phase is commonly believed to be the active catalyst in coal liquefaction and model compound pyrolysis reactions,⁷ although no specific phase has been yet been isolated as the actual catalyst species. The active iron-containing catalyst is usually generated *in situ* from an iron-oxide precursor and an elemental sulfur source under reducing conditions in the reactor vessel. Most research has concentrated on the use of common iron-oxide phases such as hematite or goethite (and their derivatives) as the iron-bearing precursor, or on non-specific iron materials produced by the reaction of various iron salts and compounds in the coal or liquefaction reactor. To our knowledge there has been no systematic effort to determine the optimum iron-containing precursor phase for producing active coal liquefaction catalysts, despite the fact that there are over ten iron-(hydroxy)oxide phases which can be easily synthesized in the laboratory.⁸

We have undertaken a systematic study to identify the most active iron-oxide catalyst precursor phases, the co-catalysts, and the coal pretreatments which will provide optimum yields in coal liquefaction processes. In this paper we present recent results of a study using a range of different authentic single phase iron-containing powders as catalyst precursors in coal model compound dissociation reactions. We also present the results of using ultrafine iron-containing powders synthesized by the Rapid Thermal Decomposition of Solutes (RTDS)^{9,10} and Modified Reverse Micelle (MRM)¹¹ methods as precursors for catalysts in model compound reactions. Preliminary results of coal liquefaction runs using both fixed volume tubing bomb reactors and a flow through micro-liquefaction reactor are included.

EXPERIMENTAL

The synthesis of iron-containing powders using MRM¹¹, RTDS,^{9,10} and standard laboratory procedures⁸ has been described elsewhere. All iron-containing materials synthesized for use in this study were analyzed by X-ray diffraction (XRD) and other methods as appropriate. The model compound (naphthyl bibenzylmethane), its synthesis, and the test reactor conditions were also described previously.^{11,12}

Tubing Bomb Coal Liquefaction Runs - Coal liquefaction studies were performed using the Wyodak and Blind Canyon Seam Argonne premium coals. The coal (1.2 g), iron-oxide catalyst precursor (0.01 g), and elemental sulfur (0.01 g) were loaded into 316 stainless steel tube reactors with 2 ml of tetralin and pressurized with 800 psi hydrogen. The total volume of the stainless steel vessel and the gas inlet was less than 6 ml. The vessels were placed in a fluidized sand bath at the selected temperature for a specified time. A thermocouple was placed in contact with the metal surface of the reactor, allowing indirect observation of the reaction temperature. The warmup times were typically 1 minute to 380°C, 5 minutes to 390°C and 10 minutes to 400°C. The temperature variation during an hour long run was $\pm 3^\circ\text{C}$ once the reaction temperature was attained.

The reaction product was extracted with tetrahydrofuran (THF), and the dried insoluble residue was used to calculate the liquefaction yield. The THF extract was reduced in volume and precipitated with pentane to determine the amount of pentane insolubles. The pentane soluble fraction was calculated by difference. All yields are reported as moisture and ash free (maf).

Micro-Liquefaction Reactor - The micro-liquefaction reactor (Fig. 1) consisted of an in-line filter assembly attached to a HPLC pump and a capillary restrictor at the reactor exit for maintaining pressure. The stainless steel fritted cup was filled with the coal or coal/catalyst mixture, weighed, and sealed inside the micro-reactor body. Tetralin was pumped at 0.2 ml per minute through the assembly at a pressure sufficient to maintain the tetralin as a liquid at 400°C. The assembly was immersed in a fluidized sand bath at the desired temperature for the appropriate time. The dark colored tetralin fractions were collected continuously. After removal from the sand bath, tetrahydrofuran was pumped through the cooled micro-reactor until the color of the effluent was a light yellow. The coal residue was weighed after Soxhlet extraction with THF and drying. After cooling, the tetralin insolubles were filtered and weighed. Pentane was then added to the THF soluble fraction to precipitate the pre-asphaltenes, which were also filtered and weighed.

RESULTS

Table I shows that most of the authentic laboratory-prepared oxyhydroxides, particularly lepidocrocite ($\gamma\text{-FeOOH}$) and goethite ($\alpha\text{-FeOOH}$), were better catalyst precursors than the oxides for carbon-carbon bond scission in naphthyl bibenzylmethane. Pure magnetite (Fe_3O_4) and maghemite ($\gamma\text{-Fe}_2\text{O}_3$) were found to be particularly poor catalyst precursors for this reaction. The proto-oxyhydroxide, 2-line ferrihydrite, was also determined to be a poor catalyst precursor for the model compound reaction. The organic products of the catalytic runs were almost exclusively methylbibenzyl and naphthalene (with some tetralin). The iron-containing products, while not rigorously characterized after the reaction runs, were typically observed as black solids with at least some ferromagnetic component.

Significant increases in the activity of the 2-line ferrihydrite, magnetite, and maghemite phases toward carbon-carbon bond scission in the model compound were noted when the materials were produced by the RTDS and the MRM methods (Table II). This increase in yields may have been due to smaller particle size or the presence of undetectable active phases in the initial catalyst precursors of the RTDS and MRM powders.

Selected coal liquefaction results utilizing tubing bombs (Table III) and using a MRM synthesized "iron-sulfide" catalyst showed that the reactivity of this catalyst appeared to change with the coal utilized. The results obtained using Wyodak coal showed an obvious improvement in both the THF soluble and the pentane soluble fractions obtained using this catalyst. There was, however, no statistical difference between the catalyzed and uncatalyzed runs when the Blind Canyon Seam coal was used with the MRM "iron-sulfide" catalyst.

The results of testing 2-line ferrihydrite catalyst precursors synthesized by the MRM method on both Wyodak and Blind Canyon Seam coals shown in Table IV. Again, a larger enhancement in the production of THF soluble products over thermal-only runs was noted when using the catalyst on the Wyodak coal. There was also an increase observed in the production of the pentane soluble fraction for both coals over the thermal-only runs when using the 2-line

ferrihydrate precursor.

Table V shows the Blind Canyon Seam coal liquefaction run results for a series of iron-oxides and oxyhydroxides produced by the RTDS method. A moderate increase in the total liquid products as well as a smaller increase in pentane solubles was observed with these catalyst precursors relative to the thermal-only run.

Figure 2 shows the liquefaction yields from Blind Canyon Seam coal when a 2-line ferrihydrate catalyst precursor produced by MRM was used in the flow-through micro-reactor. The total liquid yield in these runs was only slightly greater than in the non-catalyzed or sulfur-only thermal runs for this coal, but a definite difference was observed in the types of products formed when the flow-through reactor was used. The amounts of tetralin insolubles and pentane insolubles obtained in the catalyzed runs were significantly less than in the uncatalyzed runs.

SUMMARY

The testing of authentic iron-(hydroxy)oxide phases with the naphthyl bibenzylmethane model compound demonstrated large differences in catalytic activity between the starting iron-containing species. Materials produced by MRM and RTDS promoted more reaction with the model compound than did the phases synthesized using literature procedures. Our testing with coals showed that ultrafine iron-oxyhydroxide powders produced by the RTDS and MRM methods were good catalyst precursors for coal liquefaction in the presence of sulfur.

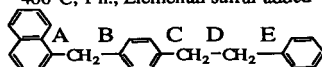
ACKNOWLEDGEMENTS

We thank Drs. J. A. Franz, D. M. Camioni and S. T. Autrey for discussions of the model compound and coal liquefaction results. We also thank the Department of Energy, Office of Fossil Energy for supporting this work under contract DE-ACO6-76RLO 1830.

REFERENCES

1. Pacific Northwest Laboratory is operated for the U. S. Department of Energy by Battelle Memorial Institute. This work was supported by the U. S. Department of Energy, Office of Fossil Energy under contract DE-ACO6-76RLO 1830.
2. Pradhan, V. R.; Tierney, J. W.; Wender, I.; and Huffman, G. P., *Energy & Fuels*, **1991**, *5*, 497.
3. Pradhan, V. R.; Herrick, D. E.; Tierney, J. W.; and Wender, I., *Energy & Fuels*, **1991**, *5*, 712.
4. Suzuki, T.; Yamada, H.; Yunoki, K.; and Yamaguchi, H., in *Proceedings: 1991 International Coal Symposium*, **1991**, 703.
5. Miki, K.; Yamamoto, Y.; Inabe, A.; and Sato, Y., in *Proceedings: 1991 International Coal Symposium*, **1991**, 675.
6. Bi, X-X; Derbyshire, F. J.; Eklund, P. C.; Hager, G. T.; and Stencel, J. M. *Energy & Fuels*, **1991**, *5*, 683.
7. Wei, X.-Y.; Ogata, E.; Aong, Z.-M.; and Niki, E. *Energy & Fuels*, **1992**, *6*, 868.
8. Schertmann, U. and Cornell, R. M. *Iron Oxides in the Laboratory*, Weinheim: New York, **1991**.
9. Mason, D. W.; Linehan, J. C.; and Bean, R. M. *Mater. Lett.*, **1992**, *14*, 222.
10. Matson, D. W.; Linehan, J. C.; and Darab, J. G. "Preparation of Ultrafine Catalyst Powders Using a Flow-Through Hydrothermal Process", This preprints.
11. Linehan, J. C.; Bean, R. M.; Matson, D. W.; Fulton, J. L.; and Crump, A. E. in *Preprints, Div. of Fuel Chem., American Chemical Society*, **1992**, *37*, 488.
12. Farcasiu, M. and Smith, C. *Energy & Fuels*, **1991**, *5*, 83.

TABLE I
 MODEL COMPOUND REACTIONS
 WITH AUTHENTIC IRON CONTAINING PHASES
 400°C, 1 h., Elemental sulfur added



Naphthyl Bibenzylmethane

Catalyst	% Consumption	Selectivity ^a
Controls		
None	2-5%	40-60%
Sulfur Only	5-20%	50-70%
Proto-Oxyhydroxide		
2-Line Ferrihydrite	7%	71%
Oxyhydroxides (FeOOH)		
Feroxyhyte (δ)	45%	90%
Akaganeite (β)	14%	97%
Lepidocrocite (γ)	70%	93%
Goethite (α)	73%	92%
Oxides		
Hematite (α-Fe ₂ O ₃)	37%	81%
Maghemite (γ-Fe ₂ O ₃)	14%	86%
Magnetite (Fe ₃ O ₄)	16%	54%

a) Selectivity is defined as [Products A + B Cleavage]/[Total Products]

Table II
 MODEL COMPOUND RESULTS
 WITH IRON-CONTAINING MATERIALS
 PRODUCED BY RTDS AND MRM METHODS
 400°C, 1 h., S added

Catalyst	% Consumption	Selectivity
Controls		
None	2-5%	40-60%
Sulfur Only	5-20%	50-70%
RTDS		
79-1 2-Line Ferrihydrite	49%	95%
79-4 Hematite	23%	83%
MRM		
39-39 2-Line Ferrihydrite	38%	90%
7-2 2-Line Ferrihydrite	51%	91%
7-2A Magnetite/Maghemite	77%	89%
9-2 "Iron-Sulfide"	68%	96%

Table III
Coal Liquefaction Results Using
MRM-Derived "Iron-Sulfide" Catalyst Precursor and Sulfur.^a

Coal	Catalyst	% THF Soluble	% Pentane Soluble
Wyodak	None	71	39
Wyodak	9-2	85	46
BCS ^b	None	83	28
BCS ^b	9-2	85	28

a) Reaction conditions: 800 psi H₂, 10 mg of sulfur, 400°C for 1 h.

b) BCS is Blind Canyon Seam.

Table IV
Reverse Micelle Derived 2-Line Ferrihydrite
Catalyst Precursors Reactions with Coals^a

Coal	Catalyst	Liquefaction Temperature	% THF Soluble	% Pentane Soluble
Wyodak	None	400°C	71	39
Wyodak	7-2 + S	400°C	88	64
BCS ^b	None	350°C	58	23
BCS ^b	99-1 + S	350°C	63	32
BCS ^b	99-2 + S	350°C	62	30

a) Reaction conditions: 800 psi H₂, 10 mg of sulfur, 1 h.

b) BCS is Blind Canyon Seam.

Table V
RTDS Derived Iron-Oxide Catalyst Precursors
Reactions with Blind Canyon Seam Coal^a

Coal	Catalyst ^b	% THF Soluble	% Pentane Soluble
BCS ^c	None	83	29
BCS ^c	2-Line Ferrihydrite + S	87	30
BCS ^c	2-Line Ferrihydrite + S	91	30
BCS ^c	Hematite + S	91	35
BCS ^c	Hematite + S	93	36

a) Reaction conditions: 800 psi H₂, 10 mg of sulfur, 400°C for 1 h.

b) Surface areas of catalyst precursors 180-215 m²/g as determined by BET.

c) BCS is Blind Canyon Seam.

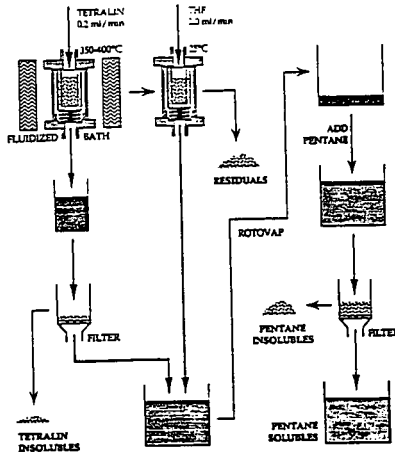


Figure 1. Schematic diagram of flow-through micro-liquefaction reactor and work-up method.

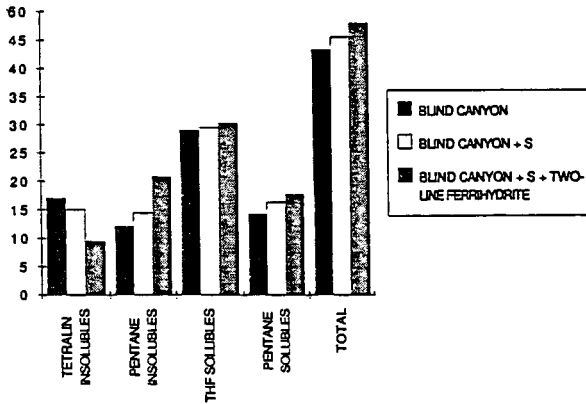


Figure 2. Liquefaction results of micro-liquefaction flow-through reactor with Blind Canyon Seam coal and a MRM synthesized 2-line ferrihydrite at 350°C for 1 hour with a 0.2 ml/min tetralin flow rate. Notice the large differences in the amount of tetralin and pentane insolubles between control and catalyzed runs.

EFFECT OF A SULFIDED, NON-POROUS AEROSOL Fe_2O_3 CATALYST ON THE
CHEMICAL STRUCTURE OF COAL LIQUIDS FROM THE
HYDROLIQUEFACTION OF A HIGHLY VOLATILE BITUMINOUS COAL

Vicente L. Cebolla¹, Moustapha Diack^{2*}, Michèle Oberson³, Robert Bacaud³, Dénise Cagniant² and Brigitte Nickel-Pépin-Donat³.

¹ Instituto de Carboquímica, CSIC. Plaza de Paraíso, 4. 50004 Zaragoza, Spain.

² Laboratoire de Chimie Organique, Université de Metz. Ile du Saulcy. 57045 Metz, France.

³ Institut de Recherches sur la Catalyse, CNRS. 2, Avenue Albert Einstein. 69626 Villeurbanne, France.

* Present address: Department of Chemistry, University of Tennessee. Knoxville, TE 37996-50.

INTRODUCTION

Previous studies related with coal liquefaction in a batch reactor demonstrated that the pertinent parameter for the activity of a dispersed catalyst is not its total surface but the accessible external surface [1]. Thus, non-porous ultrafine aerosol oxides were synthesized by combustion of the corresponding metal chlorides in a hydrogen-oxygen flame [2-4]. Iron oxide precursors obtained in this manner, and sulfided with elemental sulfur during heating, showed a high catalytic activity for a highly volatile bituminous coal even at temperatures lower than that of most bond breaking [3]. Furthermore, the sintering of the initially dispersed iron sulfide was prevented by the presence of carbonaceous solid substances [5,6].

This work was extended to other aerosol types (SnO_2 , MoO_3 , SiO_2 , Al_2O_3 , $\text{NiMo}/\text{Al}_2\text{O}_3$). Attempts were made to elucidate their active phases [7,8]. Their concentration, mode of sulfidation and introduction were also studied, as well as the effect of temperature and the solvent used [9]. Moreover, sulfided iron oxide aerosols also showed high yields in a multistage hydroliquefaction procedure [2, 10, 11].

In this paper, the effect of a sulfided aerosol Fe_2O_3 on the chemical structure of oils and asphaltenes coming from the hydroliquefaction of a highly volatile bituminous coal will be compared to the effect of the other above-mentioned aerosols. For this purpose, methods of evaluation of hydroliquefaction runs in batch reactor and analytical techniques which permit differentiation between the effects of the catalysts have been developed.

EXPERIMENTAL

Catalysts

Fe₂O₃, MoO₃ and SnO₂ aerosol precursors were obtained by combustion of the corresponding chloride vapors. They were non-porous, with particle size lower than 50 nm and with BET surfaces from 20 to 60 m²g⁻¹. SiO₂, Al₂O₃ and NiMo/Al₂O₃ were commercial aerosols from Degussa and Institut Français du Pétrole (200 m²g⁻¹ S_{BET}). More details are given in [1, 12].

Hydroliquefaction procedure

This was described elsewhere [9]. Briefly, 40 g of a high volatile bituminous coal (from Freyming, France) were suspended in tetralin (95 g) with (or without in the blank run) 2% of catalyst precursor. Elemental sulfur was added in order to obtain a partial pressure of 1% H₂S. The magnetically stirred reactor was pressurized (14 MPa) with H₂. After the heating period (3°Cm⁻¹), the nominal temperature (350, 400 or 430°C) was maintained for one hour before cooling.

Evaluation of catalytic activity in the hydroliquefaction runs

Conversions were evaluated by parallel solvent extraction with THF, toluene and n-hexane, using microfiltration under pressure as it has been described in detail [9, 13]. The results were expressed in terms of the percentage of conversion into soluble products, calculated by the difference in weight of the insoluble fractions.

The activity of catalysts in hydrogen transfer reactions was evaluated by the extent of dehydrogenation of the solvent (expressed as the ratio of naphthalene to naphthalene + tetralin, measured by gas chromatography) and by the total consumption of hydrogen gas determined by the variation of the total pressure during a run [8, 14].

The influence of the catalyst was also confirmed by measurements of Electron Spin Resonance of the stable radicals of the THF insoluble fractions. Spectra were performed in a Varian E 112 apparatus at 9 GHz. Freyming macerals had been previously isolated by Density Gradient Centrifugation [15], and ESR parameters, also obtained at 9 GHz. Assuming that inertinite is the least reactive maceral, the percentage of "destroyed" fossil radicals in inertinite after hydroliquefaction runs can be calculated. This technique has been described in depth [16].

Analytical characterization of coal liquids

Raw coal liquids were submitted to extrography [17]. A 2 g sample was dissolved in 15 ml of dichloromethane; then 16 g of activated (2 h at 120°C) silicagel were added to the solution and the mixture transferred to a column after elimination of the solvent. It was successively eluted with pentane/toluene (85/15), chloroform, chloroform/ethanol (97/3) and THF. The efficiency of extrography as a fractionation tool, advantages and structural attributions to the separated fractions have been described elsewhere [18, 19].

Derived oils and asphaltenes were separated by careful distillation of tetralin (controlled by GC/MS at 65°C under 0.27-0.4 kPa) and subsequent sequential ultrasonic extraction (Sonoclean B30 probe) in the conditions described in [20, 21].

Gas Chromatography (GC) of oils on a SE 30 glass capillary column were carried out in a Intersmat IGC 121C3 apparatus under the conditions described in [20, 21]. Identification of individual structures was out of the scope of our work. Results were summarized by retention index zones, which were calculated according to Lee et al. [22] with naphthalene,

phenanthrene and chrysene as standards. Literature reported that elution is made according to the number of total rings (aromatic or not) [23]. Index between 100-200 correspond to compounds with one ring, 200-300 to two rings, etc... This classification of ring size by retention indices can also be applied to phenolic and heterocyclic compounds, mainly nitrogen, neutral and basic compounds [23], and thiophenic structures [24].

The use of n-decane as internal standard allows a quantitative estimation (index zones) and the evaluation of non-dosed products.

Gel Permeation Chromatography (HPLC-GPC) on three μ -styragel columns in series (1 x 500 Å + 2 x 100 Å) was applied to the oils and asphaltenes in a M-600 Waters apparatus with refractive index detection using dichloromethane as eluent [20]. Qualitative interpretation of chromatograms according to the partition in four zones as a function of the retention factor (k) was carried out on the basis of 70 model compounds, as follows: $0.1 \leq k < 0.6$: "asphaltenic type" of unknown structure, $0.6 \leq k < 0.75$: alkylated aromatics, $0.75 \leq k < 0.85$: non-alkylated aromatics, and $0.85 \leq k < 1.1$: pericondensed aromatics.

RESULTS AND DISCUSSION

The evaluation of catalytic effect

At the first stage of hydroliquefaction (350°C), differentiation between the effects of the catalysts is net and related to the different conversions in preasphaltenes and asphaltenes, hydrogen consumption and percentages of stabilized fossil radicals of inertinite [3]. Fe₂O₃ and MoO₃ precursors were the most active catalysts (fig.1), also giving an enhancement of hydroaromatic structures (NMR ¹³C/CP/MAS data) and breaking of ether bridges (FTIR data) in Freyming coal [8].

Taking into account that tetralin is not dehydrogenated at this temperature, and that tetralyl radicals do not stabilize fossil radicals of inertinite, a mechanism of H₂ dissociation on catalyst surface and subsequent migration of activated hydrogen (H^{*}) to stabilize the fossil radicals of inertinite, was proposed [8]. The small size of H^{*} would allow its diffusion into the inertinite structure.

Our results show that the catalytic effect is reduced at higher temperatures and the differentiation of catalysts by the total conversion in soluble products at 400 and 430°C is somewhat indecisive, as already observed by Makabe et al. [25]. Our total conversions are comprised in all the cases between 83 and 90% [26].

The wt% of consumed H₂ is more dependent on the nature of the catalyst. Tetralin donates hydrogen in the absence of added catalyst at 400°C but when used with a catalyst, the result is an increase of the contribution of gaseous hydrogen consumption [14]. Makabe et al. [25] pointed out that thermally produced coal radicals are mainly stabilized by H^{*} when the catalyst is active. With less active catalysts, the stabilization is due to tetralin. Therefore, catalyst efficiency can be related to its ability to dissociate H₂ into H^{*} and the ratio of hydrogen transferred from gas phase to hydrogen transferred from the solvent (H_{gas}/H_{soln}) is a good test to evaluate it (table 1).

The efficiency of the catalysts (at 350 and 400°C) evaluated by H_{gas}/H_{soln} parameters, are well related to the wt% of fossil radicals stabilized in the inertinite during hydroliquefaction at the same temperatures. Table 1 shows that trends are similar for both parameters at 350°C. The order of wt% of fossil radicals stabilized at 400°C decreases in the following order: SnO₂,

~ Fe₂O₃ ~ NiMo/Al₂O₃ > MoO₃ > SiO₂ > no catalysts. Trends are also similar to H_{gas}/H_{solv}, although this last allows a clearer differentiation among catalysts. At 430°C these ratios decrease significantly as the amount of hydrogen transferred from the solvent increases because of the thermal bond cleavage.

The influence of Fe₂O₃ precursor on the structural composition of coal-derived liquids

According to the results of extrography of the raw liquids (fig.2) [13, 26], the formation of PAHs (main constituents of F1 and F2 fractions) increases significantly as the temperature increases, at the expense of polar compounds (F4) and residues. However the differentiation, for a given temperature, between runs with or without Fe₂O₃, is not decisive using this technique, except for a small increase of the lightest compounds (F1) for Fe₂O₃ runs (400 and 430°C).

More details about the structural analyses were found when characterization of oils and asphaltenes were performed by GC on capillary columns and HPLC-GPC.

GC data, using the classification according to ring size as previously described in Experimental, revealed the higher and significant proportion of two-nuclei aromatic compounds in the oils when the runs were performed with non-porous sulfided Fe₂O₃ or MoO₃ catalyst rather than with SiO₂, SnO₂ or NiMo/Al₂O₃. This effect was found at 400 and 430°C for the iron precursor (fig 3). This fact could be attributed to hydrogenolysis of ether oxide or alkyl linkages between doubled two-ringed structures rather than to hydrocracking PAHs, all structures known to exist in the products of coal liquefaction [27]. Hypothesis of hydrocracking can be eliminated because pyrrhotite Fe_{1-x}S formed from Fe₂O₃ aerosol does not meet the requirements of hydrogenative and acid functions, needed for a hydrocracking reaction [28, 29]. The hypothesis of hydrogenolysis is supported by literature data on model compound reactions using iron oxide catalyst [30-32] and pyrrhotite [33, 34]. The possibility of a hydrodesulfurization activity of some carbon-based iron catalysts has been also reported [35] and should also be considered.

GC and HPLC-GPC data showed the important effect of temperature for oils and asphaltenes, in general, and for a given catalyst run [26]. On one hand, the wt% of non-dosed GC compounds decrease as the temperature increases (from 400 to 430°C), the cases of SiO₂ and SnO₂ being the most significant (fig. 3). On the other hand, HPLC-GPC showed that the same increase of temperature involves degradation of the heaviest components of asphaltenes (0 < k < 0.6) (fig. 4). However, this technique did not permit the observation of differences among the catalysts for a given temperature neither for oils nor for asphaltenes.

ACKNOWLEDGEMENTS

The authors wish to thank CNRS-PIRSEM for financial support, H. Charcosset (Directeur du GRECO "Hydroconversion et Pyrolyse", IRC) for his encouragement and scientific assistance, and M. Besson, and M. Lambertson for fruitful discussions.

REFERENCES

- 1 Andrès-Besson, M., Charcosset, H., Chiche, P., Davignon, L., Djega-Mariadassou, G., Joly, J.P., and Prégermain, S., *Fuel* 1983, 62, 69.
- 2 Bcaud, R., Besson, M., Brodski, D., Bussiere, P., Cagniant, D., Cebolla, V.L., Charcosset, H., Djega-Mariadassou, G., Jamond, M., Nickel, B., Oberson, M., in "Progress in Synthetic Fuels", ed. by Bemtgen J.M., Imarisio, G., Graham & Trotman,

- London, p. 9, 1988.
- 3 Charcosset, H., Bacaud, R., Besson, M., Jeunet, A., Nickel, B., and Oberson, M., *Fuel Process. Technol.* 1986, 12, 189.
 - 4 Charcosset, H., and Genard, A., in "Synthetic Fuels from Coal; Status of the Technology", ed. by Romey, P.F.M., and Imarisio, G., Graham & Trotman, London, p. 339, 1987.
 - 5 Djega-Mariadassou, G., Besson, M., Brodzki, D., Charcosset, H., Tran Vinh Huu, and Varloud, J., *Fuel Process Technol* 1986, 12, 143.
 - 6 Bacaud, R., Besson, M., Oberson, M., Brodzki, D., Bussiere, P., Charcosset, H., and Djega-Mariadassou, G., in "Catalyst Deactivation", ed. by Delmon, B., and Froment, G.P., Elsevier, Amsterdam, p. 289, 1987.
 - 7 Besson, M., Bacaud, R., Brodzki, D., Bussiere, P., Charcosset, H., Djega-Mariadassou, G., Oberson, M., and Sharma, B.K., *Fuel* 1990, 69, 35.
 - 8 Oberson, M., Ph D Thesis, University of Lyon, France, 1987.
 - 9 Besson, M., Bacaud, R., Charcosset, H., Cebolla, V.L., and Oberson, M., *Fuel Process. Technol.*, 1986, 12, 91.
 - 10 Bacaud, R., Charcosset, H., and Jamond, M., *Fuel Process. Technol.* 1990, 24, 163.
 - 11 Bacaud, R., *Fuel Process. Technol.* 1991, 28, 203.
 - 12 Vergnon, P.G., and Batis Landoulsi, H., *Ind. Eng. Chem. Prod. Res. Dev.* 1980, 19, 147.
 - 13 Tischler, R.E., and Utz, B.R., *Ind. Eng. Chem. Prod. Res. Dev.* 1983, 22, 229.
 - 14 Bacaud, R., *Applied Catalysis* 1991, 75, 105.
 - 15 Muller, J.F., Abou Akar, A., Kohut, J.P., in "Advanced Methods for Coal Characterization", ed. by Charcosset, H., assisted by Nickel, B., Elsevier, Amsterdam, p.359, 1990.
 - 16 Nickel-Pépin-Donat, B., Jeunet, A., Rassat, A., in "Advanced Methods for Coal Characterization", ed. by Charcosset, H., assisted by Nickel, B., Elsevier, Amsterdam, p. 143, 1990.
 - 17 Alula, M., Diack, M., Gruber, R., Kirsch, G., Wilhelm, J.C., and Cagniant, D., *Fuel* 1989, 68, 1330.
 - 18 Cemy, J., Sebor, G., and Mitera, J., *Fuel* 1991, 70, 857.
 - 19 Cebolla, V.L., Weber, J.V., Swistek, M., Krzton, A., and Wolszszak, Proceedings of "Coal Structure'92, Krakow, Poland, september, 1992, and submitted to *Fuel*.
 - 20 Cebolla, V.L., Bacaud, R., Besson, M., Cagniant, D., Charcosset, H., and Oberson, M., *Bull. Soc. Chim. France*, 1987, 935.
 - 21 Cebolla, V.L., PhD Thesis, University of Zaragoza, Spain, 1987.
 - 22 Lee, M., and Vassilaros, D.L., *Anal. Chem.* 1979, 51, 768.
 - 23 Lauer, J.C., Vallés, D.H., and Cagniant, D., *Fuel* 1988, 67, 1273.
 - 24 Rostal, C.E., and Pereira, W.E., *J. High Resol. Chromatogr.* 1986, 9, 328.
 - 25 Makabe, M., Ohe, S., Itoh, H., and Ouchi, K., *Fuel* 1986, 65, 296.
 - 26 Cebolla, V.L., Diack, M., Oberson, M., Bacaud, R., Cagniant, D., and Nickel-Pépin-Donat, B., *Fuel Process. Technol.* 1991, 28, 183.
 - 27 Shinn, J.H., 1985 *Int. Conf. on Coal Science*, Pergamon, Sydney, p. 738.
 - 28 Lambertson, J.L., and Guisnet, M., *Applied Catalysis* 1984, 13, 181.
 - 29 Lambertson, J.L., and Guisnet, M., *J. Chem. Res., Synop.* 224.
 - 30 Utoch, S., Hirata, T., Oda, H., and Yokokawa, C., *Fuel Process. Technol.* 1986, 14, 221.
 - 31 Cassidy, P.J., Jackson, W.R., Larkins, F.P., Herten, P.A., Rash, D., and Marshall, M., in "Advanced Topics and Applications to Fossil Fuel Energy, ed. by Petrakis, L., and

- Fraissard, J.P., D. Reidel, Dordrecht, p. 739, 1984.
- 32 Yoshimoto, I., Itoh, H., Makabe, M., and Ouchi, K., *Fuel* 1984, 63, 978.
 - 33 Montano, P.A., Lee, Y.C., Yeye-Odu, A., and Chien, C.H., *Am. Chem. Symp. Ser.*, 301, 416.
 - 34 Ogawa, T., Stenberg, V.I., and Montano, P.A., *Fuel* 1984, 63, 1660.
 - 35 Abotsi, G.M.K., and Scaroni, A.W., *Fuel Process. Technol.* 1989, 22, 107.

Table 1. Evaluation of catalytic activity in coal hydroliquefaction by ESR and hydrogen balance measurements

Catalyst	% of stabilized R.		H_{gas}/H_{soliv}	
	350°C	400°C	350°C	400°C
Without	0	60	0.83	0.33
Al ₂ O ₃	0	66	1.87	0.65
SnO ₂	19	77	6.29	7.74
Fe ₂ O ₃	52	74	8.75	8.53
MoO ₃	72	68	15.62	3.17
NiMo/Al ₂ O ₃	-	73	-	13.05

Figure 1. % of conversions (THF) of hydroliquefaction runs at 350°C.

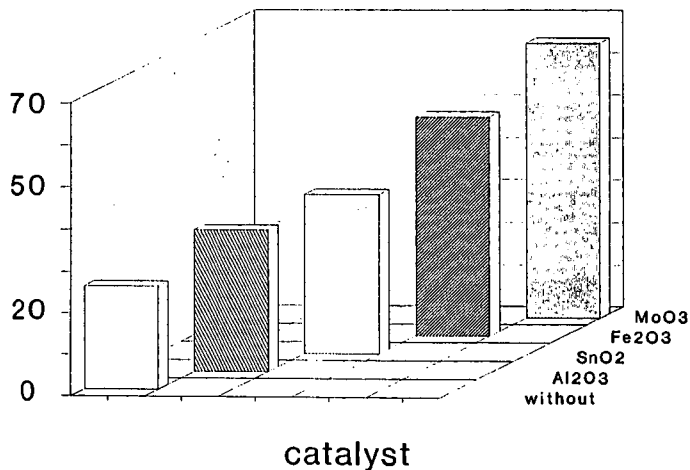


Figure 2. Iron oxide runs. Fractionation by Extrography.

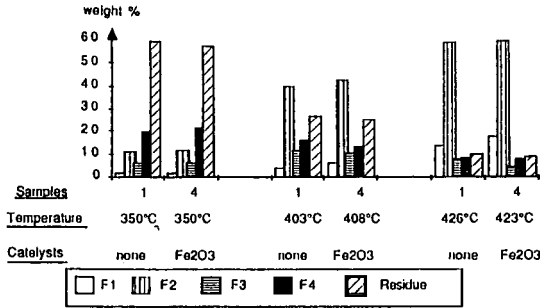


Figure 3. GC/CC analysis of oils. Classification by retention index zones.

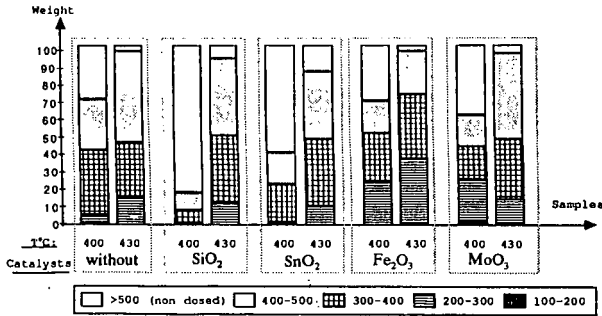
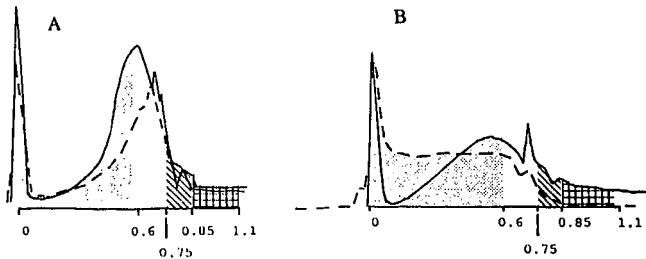


Figure 4. HPLC-GPC of oils (A) and asphaltenes (B) of iron oxide runs. (- - : 400°C; - : 430°C).



DYNAMIC STUDIES OF THE INTERACTION OF IRON SULFIDES WITH HYDROGEN

N. M. Rodriguez, and R. T. K. Baker
Materials Research Laboratory
The Pennsylvania State University
University Park, PA, 16802

Keywords: Modified iron catalysts, hydrogen spillover,
hydrogenation of solid carbon

ABSTRACT

Controlled atmosphere electron microscopy and in-situ electron diffraction techniques have been used to study the manner by which various iron sulfides interact with hydrogen using graphite as a probe material. When the metal sulfide was in direct contact or physically separated from the graphite probe, pitting of the basal plane regions was observed even at room temperature. This unusual behavior is believed to result from the action of atomic hydrogen on the metal sulfide particles. These species are extremely reactive towards the π -electrons present on the graphite basal planes and this action leads to the creation of pits. At the low pressures used in this work, 0.2 Torr, it is clear that the atomic species can migrate not only by surface diffusion processes (spillover) but also by transport through the gas phase.

INTRODUCTION

The notion of using atomic hydrogen to convert carbonaceous solids to a variety of hydrocarbon products has been the subject of a number of investigations¹⁻¹⁰. This type of study has also been extended to cover the interaction of atomic hydrogen with various coals⁶⁻¹⁰. Sanada and Berkowitz⁶ compared the reactivity pattern arising from the interaction of atomic hydrogen with various coals to that with graphite. They found that a complex mixture of gaseous hydrocarbons was produced from the coal samples, whereas when graphite was the reactant methane was the sole product. Amano and coworkers^{7,8} carried out a very comprehensive examination of the products generated from the interaction of a Japanese subbituminous coal with atomic hydrogen at 200°C and reported that gaseous hydrocarbons accounted for only 10 to 15% of the coal converted, the major product being a liquid which consisted of C₅ to C₂₂ alkanes and cycloalkanes. A somewhat different product spectrum was found by Wong and coworkers⁹ from their investigation of the reaction of atomic hydrogen with a bituminous coal (Illinois No 6), where the major products were low molecular weight volatile hydrocarbons (methane, acetylene, ethylene and propane).

Transition metal sulfides are used extensively as hydrotreating catalysts with the most important reaction in this category been hydrodesulfurization (HDS) and there are a number of excellent reviews on this subject¹¹⁻¹⁴. In such systems the precise manner by which hydrogen interacts with the sulfide catalyst is a key factor to the understanding of the mechanism. Wright and coworkers¹⁵ studied the interaction of hydrogen with alumina supported molybdenum disulfide catalysts using a combination of hydrogen adsorption and inelastic neutron scattering techniques. They found that

the uptake of hydrogen was several times higher than that which was expected from nitrogen adsorption experiments. In order to account for this unusual behavior they suggested that the adsorption of extra hydrogen could arise from intercalation into the layered structure of the sulfide particles or alternatively as a result of hydrogen "spillover" onto the alumina support.

In the current investigation we have attempted to gain a clearer understanding of the manner by which hydrogen interacts with various iron sulfides as a function of temperature by using controlled atmosphere electron microscopy techniques. In these experiments graphite has been used as a probe material since its reactivity in both molecular and atomic hydrogen is well characterized

EXPERIMENTAL

The experiments reported here were carried out in a modified JEOL 200CX TEM electron microscope, which allows one to continuously observe the behavior of a specimen as it is heated in the presence of a gas environment. In addition to being able to directly follow changes in the appearance of a specimen as it is undergoing reaction it is also possible to use the microscope in the diffraction mode and obtain information about the chemical state of the specimen at any stage of the experiment.

In this investigation two types of specimen arrangements were utilized. (a) The catalyst particles (metal sulfide) were placed in direct contact with the graphite specimen, and the observations made were limited to areas in the vicinity of the catalyst particles. (b) A microscope grid was cut in half and one section contained a pristine transmission graphite specimen and on the other, the catalyst mounted in the same manner as shown in (a). In this arrangement the catalyst and graphite probe reactant were physically separated. It was essential that when this type of specimen was placed into the environmental cell the reactant gas stream came into contact with the catalyst prior to passing over the clean graphite, the component under observation.

RESULTS AND DISCUSSION

(a) Iron Sulfide/Graphite-Hydrogen

When graphite specimens containing particulates of either FeS₂ or FeS were exposed to 0.2 Torr hydrogen a very unusual pattern of behavior was observed. Immediately following the introduction of the gas attack of the basal plane regions of the graphite support took place at room temperature. This action initially took the form of the creation of very tiny pits which became visible when their width had expanded to approximately 1.2 nm and their depths reached a level sufficient to allow a contrast difference to be observed in the transmission image between the pit and the surrounding unattacked graphite.

It was evident that in the early stages of the reaction the pits tended to be generated in clusters which were aligned in definite directions with respect to the graphite substrate. Examination of numerous areas showed that the hexagonal arrangement was predominant. On continued reaction at the same temperature the pits increased in size and in a given group gradually merged with each other to form a single larger entity up to 10 nm in width. Examination of these more highly developed pits showed

that they tended to acquire a hexagonal outline and at this stage generally contained an internal region of unattacked carbon.

The intensity of the reaction increased significantly as the temperature was gradually raised to 200°C. Unfortunately, the indiscriminate mode of attack made it impossible to identify any dynamic events that could be followed for the purposes of estimating rates of graphite hydrogenation. Moreover, the gradual deterioration in quality in the transmission image due to collection of deposit on the specimen made it difficult to resolve many surface features. In studies where the temperature was held at 350°C for extended periods of time the attack became so extensive that specimens lost their integrity and experiments were normally terminated.

On continued heating to above 500°C, the sulfide particles were observed to exhibit a change in morphological characteristics from faceted structures to a more globular geometry. This transformation which occurred at about 725°C with the iron sulfides was most clearly evident with particles located at edge regions which appeared to be quite fluid and tended to wet the graphite. This behavior was a prelude to the restoration of catalytic activity, seen as the propagation of channels by these particles when the temperature was increased by a further 100°C.

A more fundamental understanding of the factors which control the ability of a supported particle to undergo morphological changes can be obtained from a treatment of the surface forces operative at the particle-support-gas interface. Consider the situation of a metal sulfide particle located at the edge site of a carbonaceous solid exposed to a hydrogen environment, as depicted in Figure 1. The contact angle, θ at equilibrium is determined by the surface energy of the support, γ_{GS} , the surface energy of the metal sulfide particle, γ_{PG} , and the particle-support interfacial energy, γ_{PS} , and is expressed in terms of Young's equation:

$$\gamma_{GS} = \gamma_{PS} + \gamma_{PG} \cos \theta \quad (1)$$

or

$$\cos \theta = \frac{\gamma_{GS} - \gamma_{PS}}{\gamma_{PG}} \quad (2)$$

If γ_{PG} is larger than γ_{GS} , the contact angle is greater than 90° and the particle is in a non-wetting state, if the reverse is true, θ is less than 90°, then wetting occurs, and if $\gamma_{GS} = \gamma_{PS} + \gamma_{PG}$, then the particle will spread out over the support surface in the form of a thin film. Spreading of the catalyst particle results in the most efficient use of the additive in that the contact area between catalyst and carbon atoms is maximized.

The ability for particles to undergo the morphological transformations mentioned above indicates that a significant degree of atomic mobility exists, particularly in the surface layers. Previous studies¹⁶, have demonstrated that this phenomenon can occur below the Tammann temperature of the material constituting the particles, which is calculated from 0.52 [bulk melting point {K}]. For iron sulfides the Tammann temperature is about 480°C, and for systems such as those studied in this work, where a weak interaction exists with the support, particles will exhibit mobility at this temperature¹⁷.

In an attempt to determine whether the catalytic action could be sustained at even greater distances from the sulfide particles, another set of experiments was carried out

using a different specimen design. This involved complete physical separation of the supported metal sulfide and the graphite probe component. When this combination was treated in 0.2 Torr hydrogen then attack of the unadulterated graphite surface was once again observed at room temperature. In these systems, however, there was a modulation in the severity of the reaction compared to that where the catalyst and graphite were in intimate contact. It was significant to find that the incidence of pit formation showed a steady decline as one scanned across the graphite surface in the opposite direction to that where the sulfide catalyst particles were located.

A feature which must always be taken into consideration with experiments carried out within the electron microscope is whether the electron beam exerts any effect on either the gas or the solid under investigation. Concern that this problem was being encountered in the current work was dispelled by performing "blank experiments" in which specimens were reacted in hydrogen with the beam turned off for periods of up to two hours. When such specimens were eventually examined it was clear that there have been extensive reaction prior to exposure to the beam.

(b) In-Situ Electron Diffraction Analysis

In a final series of experiments the electron microscope was operated in the *in-situ* diffraction mode and patterns taken of the FeS₂/graphite specimens at various stages of the reaction during heating from room temperature up to 850°C in 0.2 Torr hydrogen. Examination of the data summarized in Table 1 shows that reduction of FeS₂ to FeS and Fe₇S₈ (Pyrrhotite) starts to occur at 240°C and at 400°C respectively, and these latter sulfides become the stable phases. At 600°C FeS appears to be the only phase present, however, on increasing the temperature to 750°C metallic iron (γ) begins to appear along with Fe₃C.

The major feature which emerges from this study is that the interaction of hydrogen with certain metal sulfides produces a species, which even at room temperature is highly reactive towards the π -electrons present on the graphite basal plane and this action leads to the creation of pits. The observation that the carbonaceous solid does not necessarily have to be in direct contact with the metal sulfide particles in order for hydro-gasification to occur, indicates that at the gas pressure used in these experiments, it is possible for the active species to be transported through the gas phase in addition to the surface migration route. The intensity of this action appears to increase with temperature up to a certain point and then come to a complete halt. Catalytic activity could, however, be regenerated by lowering of the temperature to a previously active regime.

This intriguing pattern of behavior can be rationalized according to the following arguments. At low temperature graphite can only undergo attack due to interaction with atomic species, generated from the dissociation of molecular hydrogen with metal sulfides via a reversible chemisorption process. This reaction will continue until conditions are reached which favor weakening of sulfur-metal bonds and the concomitant release of hydrogen sulfide. At higher temperatures, the sulfides are converted to the metallic state and the mode of gasification of graphite will revert to that normally associated with the metal, i.e. channeling.

ACKNOWLEDGMENTS

Financial support for this research was provided by the United States Department of Energy, Basic Energy Sciences, Grant DE-FG05-89ER14076 and CFFLS Program Contract No DE-FC22-90-PC90029.

REFERENCES

1. Blackwood, J. D., and McTaggart, F.K., *Aust. J. Chem.*, **12**, 533 (1959).
2. Gill, P. S., Toomey, R. E., and Moser, H. C., *Carbon* **5**, 43 (1967).
3. Vastola, F. J., Walker, Jr., P. L. and Wightman, J. P., *Carbon* **1**, 11 (1963)
4. Wood, B. J., and Wise, H., *J. Phys. Chem.*, **73**, 1348 (1969)
5. McCarroll, B., and McKee, D.W., *Carbon*, **9**, 301 (1971)
6. Sanada, Y., and Berkowitz, N., *Fuel*, **48**, 375 (1969).
7. Amano, A., Yamada, M., Shindo, T., and Akakura, T., *Fuel* **63**, 718 (1984).
8. Amano, A., Yamada, M., Shindo, T., and Akakura, T., *Fuel* **64**, 123 (1985).
9. Wong, C.-L. Chen, C.-W. and Timmons, R. B., *Fuel* **65**, 1483 (1986).
10. Gesser, H. D., and Czubryt, J. J., *Fuel* **67**, 375 (1988).
11. Massoth, F.E., *Adv. Catal.* **27**, 265 (1978).
12. Delmon, B., in *Proc. Climax Third Intern. Conf. on Chemistry and uses of Molybdenum* (H.F. Barry and P.C.H. Mitchell, eds) *Climax Molybdenum Co. Ann Arbor, Michigan 1980*, p 73.
13. Grange, P. *Catal. Rev. Sci. Eng.* **21**, 135 (1980).
14. Topsoe, H. and Clausen, B. S., *Catal. Rev. Sci. Eng.* **26**, 395 (1984).
15. Wright, C. J., Sampson, C., Fraser, D., Moyes, R. B., Wells, P. B. and Riekel, C., *J.C.S. Faraday I* **76**, 1585 (1980).
16. Derouane, E.G., Baker, R. T. K., Dumesic, J. A. and Sherwood, R. D., *J. Catal.* **69**, 101 (1981).
17. Baker, R. T. K., *J. Catal.* **78**, 473 (1982).

TABLE 1. IN-SITU ELECTRON DIFFRACTION ANALYSIS OF FeS₂ REACTING IN H₂

TEMPERATURE (°C)	PHASES PRESENT
240	FeS ₂ ; FeS*
300	FeS ₂ ; FeS
400	FeS ₂ ; FeS; Fe ₇ S ₈
500	FeS ₂ ; FeS; Fe ₇ S ₈
600	FeS
700	FeS
750	FeS; Fe ₃ C; α-Fe [*] ; γ-Fe

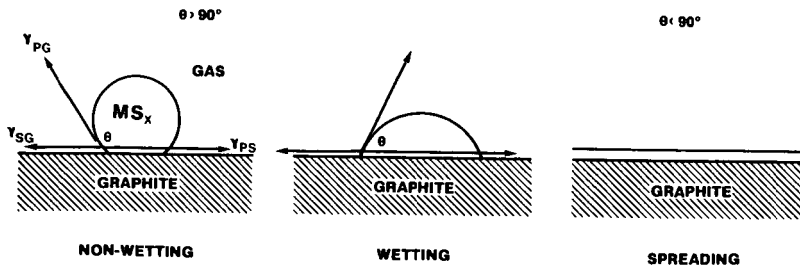


Figure 1. Metal Sulfide-Graphite-Hydrogen Interaction

* Possibly present

ACTIVITY AND SELECTIVITY OF DISPERSED IRON CATALYST IN COAL LIQUEFACTION AND MODEL COMPOUND REACTIONS

James A. Guin*, Xiaodong Zhan and Ritu Singh
Department of Chemical Engineering
Auburn University, AL 36849

Keywords: Coal liquefaction, hydrogenation, iron catalyst

INTRODUCTION

Owing to the difficulties of recovering more expensive catalysts such as Ni, Mo after use, iron has continued to be of interest as the basis of an economical and disposable catalyst for coal liquefaction. Most of the investigations on iron catalysts have focused on non-supported highly dispersed catalysts, introduced via impregnation techniques and as finely divided powder. It is believed that dispersed phase catalysts in coal liquefaction can offer several advantages over conventional ones^[2,3,6]. A suitably dispersed catalyst helps to establish a highly reducing environment with the coal matrix in the presence of hydrogen, thus reducing the need for a good hydrogen donating solvent. Effective contact of coal-solvent slurries with the catalyst surface can be achieved even at low catalyst concentration. Diffusion limitations are minimized because of the small catalyst particles. In addition, certain bond cleavage reactions can be promoted during the early liquefaction step which minimize the detrimental regressive reactions. The objective of our research is to examine the catalytic activity of dispersed iron oxide catalyst in the coal liquefaction process. To lay a good foundation for this work we have also examined the selectivity and activity of several forms of iron including Fe_2O_3 , FeS_x and reduced Fe in both a continuous and a tubing bomb microreactor (TBMR) using naphthalene and biphenyl as model compounds. Coal liquefaction experiments were also performed with a small particle iron catalyst.

EXPERIMENTAL

Coal Liquefaction Reaction Procedures: Coal liquefaction experiments were carried out in 45 cc tubing bomb microreactors (TBMR's) at the reaction conditions outlined in Table 1. The ratio of reaction solvent (tetralin, 1-methylnaphthalene, or mineral oil) to coal (Blind Canyon DECS-17 and Illinois #6) was 3:1. Elemental sulfur was added as a sulfur source with the DECS-17 coal. The iron catalyst employed was Fe-3 (Nanocat superfine iron oxide, Mach-1 Inc.). According to the product specification, it is $\alpha\text{-Fe}_2\text{O}_3$ with a surface area of $282 \text{ m}^2/\text{g}$, and particle size of 30 \AA and approximately one-half of the atoms reside on the particle surface. For each run, two horizontal TBMR's were agitated in a fluidized sand bath that was maintained at 400°C . After 60 minutes reaction time, the two TBMR's were removed and quenched in water. The pentane and THF solubles formed by coal liquefaction were measured and used as an indication of catalyst activity and liquefaction reactivity for coal samples. The equation used to calculate the pentane and THF solubles is as follows:

$$\%SOLUBLES = \frac{W_o(1-M) - (I.S. - W_c \cdot \frac{2MW_{FeS}}{MW_{Fe_2O_3}})}{W_o(1-A-M)} \cdot 100$$

W_o : initial weight of coal charged to bomb

A: fraction of ash in the coal

M: fraction of moisture in the coal

I.S.: weight of insolubles

W_c : weight of catalyst

MW: molecular weight of specified species

Model Compound Reaction Procedures: The hydrogenation activities of iron catalysts with model compounds were investigated in both tubing bomb microreactor (TBMR) and continuous reactor. Table 1 shows the TBMR experimental conditions. The two model compound systems employed were 2 wt% naphthalene (NAPH) in mineral oil (M.O.) and 2 wt% biphenyl in hexadecane. The iron catalysts were Fe-2 (Strem Chemical Inc., unsupported Fe_2O_3 powder) and Fe-3 as described earlier. CS_2 was utilized as sulfur source at 2 wt% in the liquid solution for the Fe-2 catalyst and 0.2 wt% for the Fe-3 catalyst. The catalyst loading of Fe-2 was ten times of that of Fe-3 to keep the surface area of these two catalysts about the same. The H_2 charged to the reactor was generally 1000 psig at ambient temperature. For Fe-2 catalyst, when CS_2 was added to the reactants, the initial H_2 pressure charged was increased to 1250 psig to compensate for H_2 used in converting CS_2 to H_2S . The in-situ reduction of catalysts was performed in a H_2 atmosphere for 24 hrs.

The model compound system of NAPH/M.O. and Fe-2 catalyst were tested in a CDS 900 trickle bed reactor shown schematically in Figure 1, and which has been described in detail elsewhere^[7]. The reactor was operated at 250°C and 1000 psi at a hydrogen flow rate of 100 ml/min (STP) and liquid feedstock flow rate of 0.2 ml/min. Nitrogen was used to purge and pressurize the reactor before starting the reaction.

The product samples collected from both the continuous reactor and the TBMR were analyzed with a Varian 3300 gas chromatograph. Temperature programming was used to improve peak resolution and decane used as an internal standard.

RESULTS AND DISCUSSION

Coal Liquefaction Studies

When moisture free Illinois #6 coal was used with tetralin as the reaction solvent in the tubing bomb runs, the percentage of pentane solubles (%PS) increased from 33% without catalyst to 36% with Fe-3 catalyst. For Blind Canyon coal, the %PS increased from 36% without catalyst to 44% with 2 wt.% catalyst. When sulfur was added to the coal in addition to the catalyst, the %PS increased further to 46%. This is the highest value of the pentane solubles obtained so far for any coal studied in our research.

Various other reaction solvents (e.g. mineral oil and 1-methylnaphthalene) were also used in place of tetralin; but their use did not show a significant advantage over tetralin. Figure 2 shows an overall comparison of the various reaction solvents studied. When mineral oil (a non-hydrogen donor) was used in place of tetralin, little difference was obtained between the values for pentane and THF solubles of the coals with or without catalyst. Although the use of 1-methylnaphthalene showed a similar trend as tetralin in the %PS for the coals with or without catalyst, the actual values of the %PS were somewhat lower. The percentage of THF solubles, however, increased from 74% without catalyst to 97% with catalyst. Although dispersed catalyst might be expected to reduce the influence of the reaction solvent, our study indicates that the properties of the solvent remain very significant with a dispersed catalyst.

Blind Canyon coal was used to study the effect of sintering the catalyst by preheating the catalyst alone at 400°C, 200°C, and 100°C before use. Sulfur was added to the catalyst in all liquefaction runs. The results, shown in Figure 3, show that preheating the catalyst lowers its activity presumably by lowering its surface area.

Blind Canyon coal was also used in a catalyst loading study with Fe-3 catalyst. The results, shown in Figure 4, are consistent in showing that coal conversion is increased when the number of catalytic active sites is increased; however, the effect is not great.

Model Compound Studies in TBMR In these experiments, a hydrogenation activity A_H was defined as follows to characterize the extent of hydrogenation reaction:

$$A_H = \frac{2M_T + 5M_D}{5(M_N + M_T + M_D)} \quad \text{or} \quad A_H = \frac{3M_{CHB} + 6M_{DCH}}{6(M_{BPH} + M_{CHB} + M_{DCH})}$$

Where, M_N : moles of naphthalene/gram of liquid product
 M_T : moles of tetralin/gram of liquid product
 M_D : moles of decalin/gram of liquid product
 M_{BPH} : moles of biphenyl/gram of liquid product
 M_{CHB} : moles of cyclohexylbenzene/gram of liquid product
 M_{DCH} : moles of dicyclohexyl/gram of liquid product

Fe-2 catalyst was reduced in hydrogen at 400°C, and Fe-3 catalyst was reduced at different temperatures in advance to examine the activity with naphthalene as reactant. Figure 5 showed that 200-250°C would be a suitable reduction temperature. It is likely that a higher temperature would cause the 30 Å catalyst to be sintered and thus lower the activity. Therefore, a reduction temperature of 200°C for Fe-3 was chosen for the later runs. Figure 6 indicated that, for the naphthalene hydrogenation, both the pre-reduced iron catalysts gave higher activities than their oxide forms, and sulfur almost completely poisoned both catalysts, whether in the oxide or metallic form. Similar results were obtained for the hydrogenation of biphenyl as shown in Figure 7. A notable phenomenon observed was that, in both reaction systems, secondary reactions, e.g., the conversion from tetralin to decalin, took place only when the catalysts had been reduced, even at the highest catalyst loadings. This suggests that the metallic iron is more active for

hydrogenation than iron oxide owing to active sites of greater activity rather than an increase in number of sites.

Model Compound Studies in Continuous Reactor The test results of three trickle bed reaction runs with sulfur in the feed in different periods are shown in Figure 8. It can be seen that when iron oxide was used as catalyst, without sulfur in the feed, the hydrogenation activity of NAPH increased gradually to a relatively stable level. However, once the sulfur was introduced, the A_H dropped continuously to about zero after 32 hrs during this process indicating that the hydrogenation reactions have been inhibited by the presence of CS_2 . The other two runs were performed by adding CS_2 to the feed first and then switching to the CS_2 free feed. The results (Figure 8) showed no reaction at 250°C once there was CS_2 in the feed, and A_H could not be restored. This indicates that H_2S has poisoned the iron catalyst permanently for the hydrogenation reactions and/or that the sulfide form of the iron is much less active than the hydrogen reduced form. After removal of the CS_2 in the feed at 48 and 92 hours, both runs showed very small, but stable A_H as the residual H_2S concentration in the reactor became smaller. This indicates that the FeS_x form of the catalyst has finite, although significantly lower hydrogenation activity than the H_2 reduced form of iron. The inhibition effect of H_2S is consistent with the earlier works by Rhee^[4] with NAPH hydrogenation in batch reactor using Ni-Mo/ Al_2O_3 catalyst and Sapre^[5] with biphenyl hydrogenation in the continuous reactor using Co-Mo/ Al_2O_3 catalyst.

Considering the hydrogenation behavior of NAPH over iron catalysts in both continuous reactor and TBMR, we think there probably exists a corresponding reduction process before the reaction occurs when iron oxide is employed. We suggest that the active phase of iron catalyst in the hydrogenation processes investigated in the absence of sulfur may be metallic iron. We have also reported^[1] that hydrogen reduced iron generally yields higher hydrogenation activity than the iron sulfide which is a much less active hydrogenation catalyst. However, the iron sulfide form may possess a higher cracking activity which may be more beneficial to coal liquefaction.

ACKNOWLEDGEMENTS

This work was supported by the U.S. Department of Energy Under Contract No. DE-FC22-90PC90029.

REFERENCES

1. Guin, J.A., Zhan, X., *Yearly Report to DOE*, 1992.
2. Hirschon, A.S., Wilson, R.B., *ACS Fuel Preprints*, p881,
3. Pradhan, V., Tierney, J.W., Wender, I., *ACS Fuel Preprints*, 5(3), p793, 1990.
4. Rhee, Y.W., Guin, J.A., *Fuel Processing Tech.*, 19, p1, 1988.
5. Sapre, A.V., Gates, B.C., *Ind. Eng. Chem. Process Des. Dev.*, 21, p86, 1982.
6. Utz, B.R., Cugini, A.V., Frommell, E.A., *ACS Fuel Preprints*, 34(4), p1423, 1989.
7. Wang, W.P., Guin, J.A. *Fuel Processing Tech.*, 28, p149, 1991.

Table 1. TBMR Reaction Conditions

Reactant wt. (g)	Coal 3	NAPH 0.24		BPH 0.24
Catalyst wt. (g)	Fe-3 0.66	Fe-2 0.6	Fe-3 0.06	Fe-3 0.06
Solvent wt. (g)	Tetralin etc. 10	Mineral Oil 12	Mineral Oil 12	Hexadecane 12
Sulfur Source wt. (g)	Elementary Sulfur 0.1	CS ₂ 0.24	CS ₂ 0.024	CS ₂ 0.024
Temp. (°C)	400	350	350	300
H₂ Pressure (psi)	1250	1000 (1250)	1000	1000
Time (h)	1	1	1	1

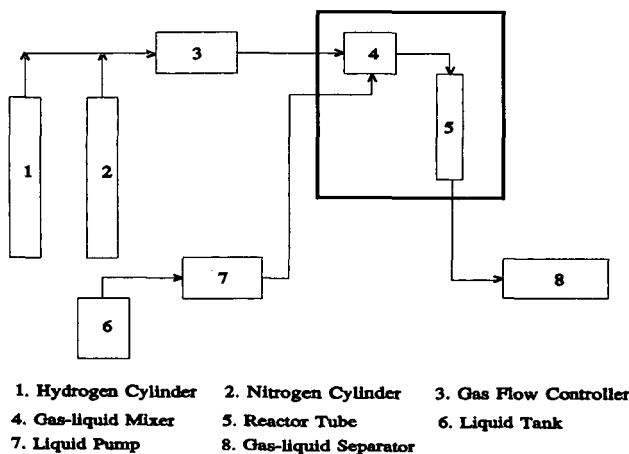


Figure 1. CDS 900 Reactor System

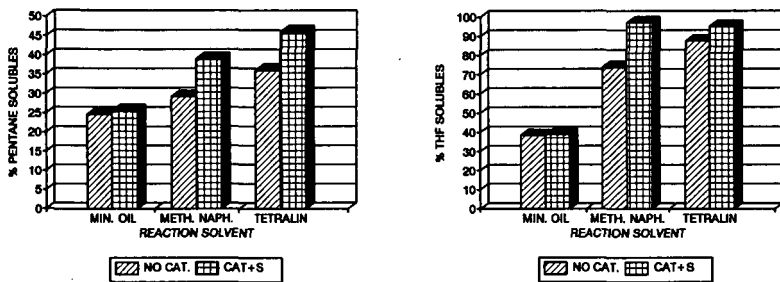


Figure 2. Comparison of Reaction Solvents using Blind Canyon Coal

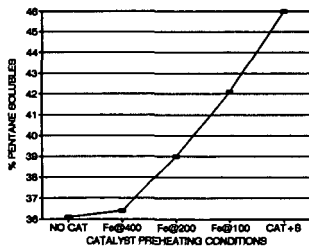


Figure 3. Effect of Preheating the Catalyst at Different Temperatures

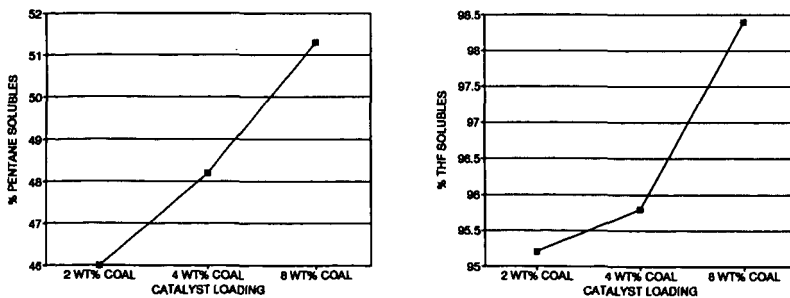


Figure 4. Comparison of Different Loadings of Catalyst

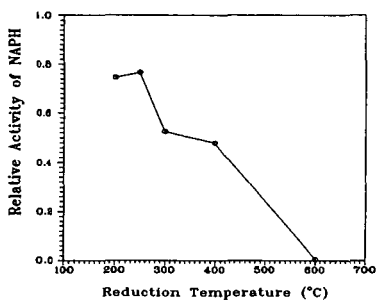


Figure 5. Effect of Reduction of Fe-3 Catalyst at Different Temperatures on NAPH Activity in TBMR

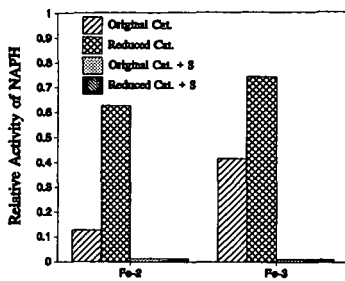


Figure 6. NAPH Hydrogenation Activity at 350 °C in TBMR

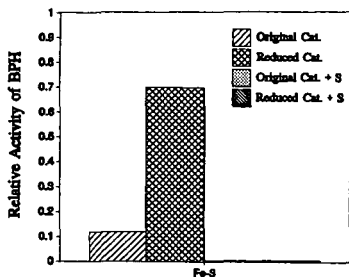


Figure 7. BPH Hydrogenation Activity at 300°C in TBMR

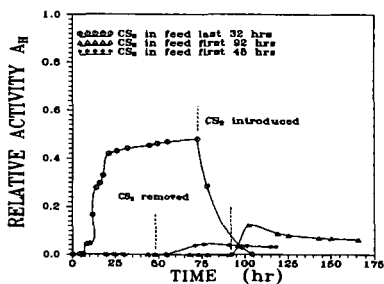


Figure 8. NAPH Hydrogenation Activity at 250°C in Continuous Reactor